

Journal Pre-proof

The most primitive CM chondrites, Asuka 12085, 12169, and 12236, of subtypes 3.0–2.8: Their characteristic features and classification

M. Kimura, N. Imae, M. Komatsu, J.A. Barrat, R.C. Greenwood, A. Yamaguchi, T. Noguchi



PII: S1873-9652(20)30074-8

DOI: <https://doi.org/10.1016/j.polar.2020.100565>

Reference: POLAR 100565

To appear in: *Polar Science*

Received Date: 19 April 2020

Revised Date: 26 July 2020

Accepted Date: 6 August 2020

Please cite this article as: Kimura, M., Imae, N., Komatsu, M., Barrat, J.A., Greenwood, R.C., Yamaguchi, A., Noguchi, T., The most primitive CM chondrites, Asuka 12085, 12169, and 12236, of subtypes 3.0–2.8: Their characteristic features and classification, *Polar Science* (2020), doi: <https://doi.org/10.1016/j.polar.2020.100565>.

This is a PDF file of an article that has undergone enhancements after acceptance, such as the addition of a cover page and metadata, and formatting for readability, but it is not yet the definitive version of record. This version will undergo additional copyediting, typesetting and review before it is published in its final form, but we are providing this version to give early visibility of the article. Please note that, during the production process, errors may be discovered which could affect the content, and all legal disclaimers that apply to the journal pertain.

© 2020 Elsevier B.V. and NIPR. All rights reserved.

1 **The most primitive CM chondrites, Asuka 12085, 12169, and 12236, of**
2 **subtypes 3.0-2.8: Their characteristic features and classification**

3

4 M. Kimura^{1,*}, N. Imae¹, M. Komatsu², J. A. Barrat³, R. C. Greenwood⁴, A. Yamaguchi¹, and T.
5 Noguchi⁵

6 ¹National Institute of Polar Research, Tokyo 190-8518, Japan, ²SOKENDAI, Kanagawa 240-0193,
7 Japan, ³Université de Bretagne Occidentale, Institut Universitaire Européen de la Mer, CNRS
8 UMR 6538, Place Nicolas Copernic, 29280 Plouzané, France, ⁴Planetary and Space Sciences, The
9 Open University, Milton Keynes MK7 6AA, United Kingdom, ⁵Kyushu University, Fukuoka
10 819-0395, Japan.

11 * Corresponding author, kimura.makoto@nipr.ac.jp

12

13 **Abstract**

14 CM chondrites (CMs) are the most abundant group of carbonaceous chondrites. CMs
15 experienced varying degrees of secondary aqueous alteration and heating that modified or
16 destroyed their primitive features. We have studied three chondrites, Asuka (A) 12085, A 12169,
17 and A 12236. Their modal compositions, chondrule size distributions, and bulk composition
18 indicate that they are CMs. However, the common occurrence of melilite in CAIs and glass in
19 chondrules, abundant Fe-Ni metal, the absence of tochilinite-cronstedtite intergrowths, and almost
20 no phyllosilicates, all suggest that these chondrites, especially A 12169, experienced only minimal
21 aqueous alteration. The textures and compositions of metal and sulfides, the lack of ferroan rims
22 on AOA olivines, the compositional distribution of ferroan olivine, and the Raman spectra of their
23 matrices, indicate that these chondrites experienced neither significant heating nor dehydration.

24 These chondrites, especially A 12169, are the most primitive CMs so far reported. The degree of
25 the alteration increases from A 12169, through A 12236, to A 12085. We propose the criteria for
26 subtypes of 3.0-2.8 for CMs. A 12169, A 12236, and A 12085 are classified as subtype 3.0, 2.9,
27 and 2.8, respectively. The oxygen isotopic composition of the Asuka CMs is consistent with these
28 samples having experienced only a limited degree of aqueous alteration. The CM and CO groups
29 are probably not derived from a single heterogeneous parent body. These chondrites are also of
30 particular significance in view of the imminent return of sample material from the asteroids Ryugu
31 and Bennu.

32

33 Keywords: Meteorites, Carbonaceous chondrite, Classification, Oxygen isotopes, CM2 CO3
34 precursors

35

36

37 **1. Introduction**

38 Carbonaceous (C) chondrites are some of the most primitive materials in the solar system, and
39 are classified into eight major chemical groups, CI, CM, CO, CV, CR, CH, CB, and CK (e.g.,
40 Weisberg et al., 2006). The CMs are the most abundant group of C chondrites (after Krot et al.,
41 2014) and appear to be widely distributed within the inner solar system, occurring as brecciated
42 fragments and clasts in a wide range of meteorite types (e.g., Zolensky et al., 1996).

43 All known CMs have lost their primitive features because of aqueous alteration and/or
44 secondary heating (e.g., Rubin et al., 2007; Nakamura, 2005), with the notable exception of the
45 CMs that are the focus of this work, based on the preliminary results of Kimura et al. (2019). Some
46 weakly altered CM and related chondrites have been recently reported, such as Paris (Hewins et al.,

47 2014), EET 96029 (Lee et al., 2016), NWA 5958 (Jacquet et al., 2016), LEW 85311 (Lee et al.,
48 2019), and NWA 11024 (Ebert et al., 2019). However, their primitive features before alteration are
49 not completely preserved in them. Recently, Yamaguchi et al. (2016) reported the recovery of
50 three CMs, Asuka (A) 12085, A 12169, and A 12236. Here we report the petrography, mineralogy,
51 bulk chemistry and oxygen isotope composition of these chondrites, to explore their characteristic
52 features, classifications, and precursor materials.

53 We will conclude that these three Asuka chondrites are CMs and that they are amongst the
54 most primitive members of this group so far reported. These chondrites provide important
55 information about the primitive features of CMs before the secondary processes in their parent
56 body. We propose subtypes 3.0-2.8 for CMs, modified from Rubin (2015).

57

58 **2. Samples and experimental methods**

59 The joint expedition party between Japan and Belgium (JARE-54 and BELARE 2012-2013)
60 collected 420 meteorites from the Nansen Ice Field, Antarctica (Imae et al., 2015). A 12085, A
61 12169, and A 12236 are included in this collection and were recovered in a 7km x 2km area of the
62 area B (Imae et al., 2015). The original (recovered) weights of A 12085, A 12169, and A 12236
63 were 9.114, 2.264, 93.65 g, respectively. For this study, we have examined the polished thin
64 sections, A 12085,41-1, A 12169,31-1, and A 12236,51-1. The area of these sections are 151.9,
65 42.0 and 98.1 mm², respectively.

66 In order to compare these chondrites with the other C chondrites, we also analyzed A 12248
67 (CM2.0), Murchison (CM2.5), ALH-77307 (CO3.03), and Y-81020 (CO3.05).

68 Back-scattered electron (BSE) images were obtained using the JEOL JSM-7100F field
69 emission scanning electron microscope (FESEM) at the National Institute of Polar Research

70 (NIPR). We conducted mineral analyses using the JEOL JXA8200 electron-probe microanalyzer
71 at NIPR, with a focused beam, and 10-30 nA beam currents for silicate phases and 30 nA beam
72 current for opaque minerals. All these analytical methods have been previously described by
73 Yamaguchi et al. (2011). The matrix was measured by using a defocused beam (5 μm in diameter)
74 for ~100-200 randomly selected points that avoided coarse-grained silicate and opaque minerals to
75 calculate an average bulk matrix composition. The elemental X-ray maps of the whole thin
76 sections were obtained using the FESEM. We obtained the modal compositions of the sections
77 from the elemental maps, using ImageJ software.

78 We identified some phases using a laser micro Raman spectrometer (JASCO NRS-1000)
79 using 532-nm excitation at the NIPR, after the method of Kimura et al. (2017). Raman spectra for
80 D- and G-bands were also collected on randomly-selected matrix areas on the sections after the
81 method of Komatsu et al. (2018). Imae et al. (2019) have recently applied an X-ray diffraction
82 (XRD) method to characterize minerals in meteorite thin sections by using SmartLab, RIGAKU at
83 the NIPR. We used the same method for the samples studied here, although the silicon 100 index
84 wafer with the opening 8 mm in diameter and the 125 μm thickness was used in this study, to
85 reduce the diffraction from epoxy resin surrounding the sample. The accuracy of the diffraction
86 angle is within 0.02°. Isolated peaks for a phase were used, which do not overlap with the other
87 phases. We use only intense peaks for phase identification, and they are normally 1000-10000
88 counts much higher than the background level. We did not use the other lower peaks because of
89 the ambiguous identification of peaks.

90 Trace elements for A 12236, the largest among samples studied here, were determined by
91 ICP-SFMS and ICP-AES using the same procedure as Barrat et al. (2012) and Kimura et al.
92 (2014).

93 The bulk oxygen isotope compositions of A 12085, A 12169 and A 12236 were determined
94 by infrared laser-assisted fluorination at the Open University (Miller et al., 1999; Greenwood et al.,
95 2017). Whole-rock powders of the three CMs were prepared by crushing and homogenizing
96 approximately 100 mg fresh interior chips for each of the samples.

97 Due to their relatively high phyllosilicate contents, CM chondrites can be challenging
98 samples to analyse by laser fluorination. This is essentially because the normal blank reduction
99 procedure, which involves flushing the chamber with aliquots of BrF₅, may lead to the preferential
100 reduction of the hydrated silicate fraction prior to analysis. To minimise this problem, A 12085, A
101 12169 and A 12236 were all run in “single shot” mode, with only one standard and one 2 mg
102 sample aliquot loaded in the sample chamber at a time. Further details of the “single shot”
103 procedure are given in Lee et al. (2019).

104 Analytical precision (2σ) for the Open University system, based on replicate analyses of an
105 internal obsidian standard, is ±0.053‰ for δ¹⁷O; ±0.095‰ for δ¹⁸O; ±0.018‰ for Δ¹⁷O (2σ)
106 (Starkey et al., 2016). Oxygen isotopic analysis for the three CMs are reported in standard δ
107 notation, where δ¹⁸O has been calculated as: $\delta^{18}\text{O} = [({}^{18}\text{O}/{}^{16}\text{O})_{\text{sample}}/({}^{18}\text{O}/{}^{16}\text{O})_{\text{ref}} - 1] \times 1000$ (‰)
108 and similarly for δ¹⁷O using the ¹⁷O/¹⁶O ratio, the reference being VSMOW: Vienna Standard
109 Mean Ocean Water. For the purposes of comparison with the results of Clayton and Mayeda (1999)
110 Δ¹⁷O, which represents the deviation from the terrestrial fractionation line, has been calculated as:
111 $\Delta^{17}\text{O} = \delta^{17}\text{O} - 0.52 \times \delta^{18}\text{O}$.

112

113 3. Results

114 3.1 Petrography

115 3.1.1 Overall features and modal compositions

116 A 12085, A 12169, and A 12236 show typical C chondritic textures, mainly consisting of
117 chondrules, refractory inclusions, isolated silicates and opaque minerals, and matrix (Fig. 1). None
118 of these chondrites show brecciated textures, but some clasts are encountered in A 12085 and
119 12169. Figure 1c shows that Ca-Al-rich inclusions (CAIs) are common in A 12169.

120 Table 1 compares the modal abundances of the Asuka chondrites with weakly altered CMs
121 whose detailed modal data are known. The most abundant component is the matrix, followed by
122 chondrules in the Asuka chondrites (Table 1). The modal abundances of chondrules with isolated
123 silicate minerals are 29 - 39 vol. % and those of matrices are 53 - 65 %. They are within the ranges
124 for CMs (Weisberg et al., 2006). The abundances of refractory inclusions are 3.8 - 4.3 vol.%. One
125 of the distinct features of these chondrites is the abundant occurrence of Fe-Ni metal, 1.2 - 2.3
126 vol.% (Table 1). The abundances of metal are much higher than those (<1.2 vol.%) in CM2.7-2.0
127 (Rubin et al., 2007; Rubin, 2015). Sulfide minerals are also abundant, 0.9-1.4 vol.%, in these
128 chondrites.

129 These chondrites have experienced only very low levels of shock metamorphism (shock stage
130 1) or terrestrial weathering (A) (Yamaguchi et al., 2016). A 12169 section has fusion crusts (below
131 ~1.5 mm in width).

132

133 3.1.2 Refractory inclusions

134 Refractory inclusions are easily recognizable in these chondrites. The sizes of the refractory
135 inclusions are smaller than ~300 μm . Many CAIs are surrounded by rims, consisting mainly of
136 high-Ca pyroxene (Fig. 2a). The CAIs commonly consist of spinel, melilite, and high-Ca pyroxene,
137 with a minor amount of perovskite and grossite. Melilite is abundant in the CAIs. Melilite-bearing
138 CAIs are 70, 60, and 20% of all CAIs in A 12169, A 12236, and A 12085, respectively, although

139 spinel-pyroxene CAIs are predominant in A 12085. Secondary alteration minerals, such as
140 phyllosilicate, nepheline, sodalite, and hedenbergite, are not encountered in these CAIs.

141 Amoeboid olivine aggregates (AOAs) are also common in these chondrites. The AOAs
142 mostly consist of forsteritic olivine, with minor amounts of spinel, anorthite and high-Ca pyroxene
143 intergrown with olivine grains (Fig. 2b). The AOA olivines do not have visible FeO-rich rims.
144 AOAs in these meteorites do not contain any secondary minerals, as was also the case for the
145 CAIs.

146

147 3.1.3 Chondrules and isolated silicate minerals

148 Sharply delineated chondrules are an abundant component in these chondrites (Fig. 2c). Table
149 2 summarizes the characteristic features of the chondrules. Their apparent average diameter, ~0.3
150 mm, is typical of CMs (Weisberg et al., 2006).

151 Porphyritic chondrules are the most common type, with a few barred chondrules also present
152 (Table 2). The abundances of radial and cryptocrystalline chondrules are below 3%. Type I
153 chondrules, ~90 % of all chondrules, are much more abundant than type II. The relatively high
154 abundance of type I, compared to type II chondrules, is a characteristic feature of CM chondrites.
155 Most porphyritic chondrules, especially type Is, consist of olivine and low-Ca pyroxene, with
156 minor amounts of high-Ca pyroxene, feldspar, and a spinel group mineral. Olivine, low-Ca
157 pyroxene, and often high-Ca pyroxene are phenocryst phases in chondrules (Fig. 2d). Low-Ca
158 pyroxene is identified as clinoenstatite, based on optical microscopic observations. Feldspar is an
159 abundant mesostasis phase (Fig. 2c) and does not always show a devitrified texture when
160 intergrown with high-Ca pyroxene. Porphyritic chondrules also contain a glassy mesostasis,
161 especially in some of the chondrules of A 12169 (Fig. 2d). Feldspar and glass are the primary

162 mesostasis phases, like those in type 3 chondrites. The secondary anhydrous phases, such as
163 nepheline and hedenbergite, found in the other C chondrites (e.g., Kimura and Ikeda, 1995), are
164 not encountered. Type II chondrules contain abundant ferroan olivine, often with forsteritic olivine
165 relicts (Fig. 2e). Chondrules, especially in A 12085 and A 12236, are commonly surrounded by
166 fine-grained rims (Fig. 2e).

167 Olivine and pyroxene grains in chondrules do not display secondary diffusional zoning nor
168 the phyllosilicate veinlets that are common in the more altered CMs (Lee and Lindgren, 2016).
169 Clinostatite grains do not show alteration features along their twin boundaries.
170 Tochilinite-cronstedtite intergrowths (TCI) do not present in the chondrules of these meteorites, in
171 clear contrast to most other CMs.

172 Phyllosilicates are sometimes encountered within the outer margins of some A 12169
173 chondrules, whereas they commonly occur throughout the chondrules in A 12085 (Fig. 2f). A
174 12236 shows features that are intermediate between A 12169 and A 12085. On the other hand,
175 primary mesostasis, unaltered feldspar and glass are commonly present in A 12169 chondrules.
176 These phases are also present in some chondrules from A 12236, but are uncommon in A 12085.
177 We examined 50 chondrules selected from each chondrite, and divided them into chondrules with
178 completely altered (no primary mesostasis), partly altered, and unaltered mesostasis (only primary
179 mesostasis). The abundances of unaltered mesostasis-bearing chondrules decreases from A 12169,
180 through A 12236, to A 12085 (Table 2).

181 Chondrules commonly contain Fe-Ni metal spherules which are usually kamacite as
182 mentioned later. They occur within and at the outer margins of chondrules. These metals are
183 mostly homogeneous in texture (Fig. 2g). Plessitic intergrowth, noticed in Semarkona (LL3.01)
184 (Kimura et al., 2008), is not present.

185 In addition to chondrules, isolated silicate grains, less than several tens microns in size, are
186 abundantly encountered in the matrices. They are mostly fragmental in shape and are
187 predominantly olivine and low-Ca pyroxene. They are also unaltered. Their mineralogy,
188 composition and fragmental morphology indicates that most of these grains were derived by
189 disaggregation and disruption of chondrules.

190

191 3.1.4 Matrix

192 Figure 2h shows a matrix area of A 12169. The matrix mostly consists of fine-grained silicate
193 phases of submicron size. Fe-Ni metal and Fe-sulfides, less than 150 μm in size, occur as isolated
194 grains in the matrix. The Fe-sulfides are mostly troilite. Rare pentlandite is always present in
195 association with isolated pyrrhotite grains (Fig. 2i). In addition to these larger-sized opaque
196 minerals, fine-grained opaque minerals, submicron in size, are abundantly mixed with silicate
197 phases in the matrix (Fig. 2h).

198 No TCI was observed in the matrices of these chondrites. However, aggregates of
199 Fe-sulfide(s) mixed with silicate phases of submicron size (Fig. 2j) are present, especially in A
200 12085. They are not common in A 12169.

201

202 3.2 Mineralogy

203 3.2.1 Olivine

204 Table 3 shows selected analyses of silicate and oxide phases. Olivine is common in
205 chondrules, in matrix as isolated grains, and in AOAs. Olivine in type I and II chondrules is
206 Fo_{92-100} and Fo_{30-88} , respectively, although some type II chondrules contain relict forsterite grains
207 ($\text{Fo}_{<99}$). Olivines in chondrules contain <0.69 wt.% Cr_2O_3 , <0.68 wt.% MnO , and <0.70 wt.% CaO .

208 Olivines in AOAs are Fo₉₈₋₁₀₀. Chemical zoning has not been observed in these AOAs. The
209 olivines in AOAs contain <0.46 wt.% Cr₂O₃, <0.61 wt.% MnO, and <0.35 wt.% CaO.

210 Figure 3a shows the distribution of Fe and Mn in olivines in chondrules, isolated grains, and
211 AOAs, including those in Murchison (CM2.5). All these chondrites show similar distributions.
212 This Fe-Mn distribution trend is consistent with those of ferroan olivines in CM and CO chondrites
213 (Schrader and Davidson, 2017). Olivines in some AOAs and isolated minerals show a high Mn/Fe
214 distribution trend. Such a trend is commonly observed in AOAs (e.g., Komatsu et al., 2015).

215 The average Cr₂O₃ content and standard deviation for cores of ferroan olivine grains (>2 wt.%
216 FeO) are 0.34 wt.% and 0.08, 0.35 wt.% and 0.08, and 0.32 wt.% and 0.08 for A 12085, A 12169,
217 and A 12236, respectively. These data plot within the range of those in primitive COs and some
218 CMs (Grossman and Brearley, 2005; Schrader and Davidson, 2017) (Fig. 3b).

219

220 3.2.2 Pyroxene

221 Pyroxene is the second most abundant mineral in these chondrites. It is divided into low-Ca
222 (<0.15 atomic Ca/(Ca+Mg+Fe) ratio) and high-Ca pyroxenes. Low-Ca pyroxenes are abundant in
223 type I chondrules and are magnesian (En₈₅₋₉₉Fs_{0.4-9.9}Wo_{0.3-13.1}). On the other hand, low-Ca
224 pyroxenes are minor in type II chondrules and are ferroan (En₃₈₋₇₁Fs₂₂₋₆₁Wo_{0.1-10.1}). In some
225 chondrules, Al-rich low-Ca pyroxene occurs (<14.6 wt.% Al₂O₃). Such pyroxene compositions
226 have been reported from some other chondrites, such as Semarkona (LL) (Rubin, 2004) and
227 Y-82094 (ungrouped C chondrite) (Kimura et al., 2014).

228 High-Ca pyroxenes are present in chondrules as a mesostasis phase and also as phenocrysts in
229 both chondrules and refractory inclusions. In chondrules, the high-Ca pyroxene compositional
230 range is En₄₈₋₈₃Fs_{0.5-9.7}Wo₁₆₋₄₆ in type Is and En₂₀₋₅₄Fs₁₁₋₅₆Wo₁₉₋₅₀ in type IIs. High-Ca pyroxenes

231 in refractory inclusions contain 0.8-38 wt.% Al_2O_3 , and <5.1 wt.% TiO_2 (Table 3). A pyroxene that
232 is highly enriched in Al_2O_3 , 38 wt.%, in a CAI is kushiroite (Kimura et al., 2009).

233

234 3.2.3 Feldspar and glass

235 Chondrules contain abundant feldspar or glass in their mesostasis. Feldspars are anorthositic
236 (An_{89-100}) in type I chondrules, whereas type II chondrules contain albitic feldspar (Ab_{54-77}). Cation
237 total of anorthitic feldspar ranges from 4.93-5.01, suggesting that some feldspar contain excess
238 silica component, which is reported from primitive C chondrites (e.g., Tenner et al., 2018).
239 Feldspars in refractory inclusions are always nearly pure anorthosite (An_{99-100}).

240 Chondrule glasses are enriched in feldspathic components (Fig. 4) and contain 10-33 wt.%
241 Al_2O_3 , 1.9-31 wt.% CaO , and 0.2-7.2 wt.% Na_2O . The compositions resemble those of CO
242 chondrules. The total weight percent ranges from 98.1 to 101.7, suggesting that they are not
243 phyllosilicate. The occurrence of glass has been reported only in some CMs (e.g., Ikeda, 1983;
244 Hewins et al., 2014).

245

246 3.2.4 Phyllosilicates in chondrules

247 Mesostasis in chondrules also contains phyllosilicate, and their abundance depends on the
248 chondrite as mentioned before. The average analytical total of phyllosilicate-dominated areas is
249 85.5 wt.%, which is much lower than that of matrix as mentioned later. Such total weight percent
250 supports that they are phyllosilicates. Their compositions suggest that they are mixtures of
251 serpentine and saponite (Fig. 4), and similar to those in other CMs, such as Murchison, and COs
252 (this work; Ikeda, 1983).

253

254 3.2.5 Other minor minerals

255 Melilite in refractory inclusions is enriched in the gehlenite component (Geh₇₇₋₉₉). Spinel in
256 inclusions is nearly pure MgAl₂O₄, containing only small amounts of FeO (<0.4 wt.%) and Cr₂O₃
257 (<0.7 wt.%). Type I chondrules occasionally contain Mg-Al spinel (50-71 wt.% Al₂O₃ and 0.4-5%
258 FeO wt.%), and type II chondrules contain chromite (30-55 wt.% Cr₂O₃ and 18-28 wt.% FeO).
259 Type II chondrules contain rare phosphates, most of which are no more than a few microns in
260 diameter. One of these was identified as merrillite from the composition (Table 3). Ca-carbonate is
261 observed in a few chondrules of A 12085. Small Ca-carbonate grains were also observed in a clast
262 in A 12169. Framboidal magnetite occurs in a clast in A 12085.

263

264 3.2.6 Fe-Ni metal and sulfides

265 Table 4 gives representative compositions of Fe-Ni metal and sulfides. Fe-Ni metal is divided
266 into kamacite (<7.5 wt.% Ni) and Ni-rich metal (Kimura et al., 2008). Kamacite and Ni-rich metal
267 contain <0.6 wt.% and 0.2-2.5 wt.% Co, and 0.3-7.4 wt.% and 7.5-46.5 wt.% Ni, respectively.
268 Ni-depleted metal (0.3 wt.% Ni) was found within dusty olivines in a chondrule in A 12085. From
269 the occurrence and composition, this metal seems to be a reduction product (Leroux et al., 2003).
270 Fe-Ni metal contains <1.0 wt.% Si, <2.6 wt.% P, and <1.5 wt.% Cr, which is consistent with other
271 CMs that have experienced low degrees of heating (Kimura et al., 2011). A few grains are rich in P
272 (1.9-2.6 wt.%), but phosphides do not appear to be present. A positive correlation exists between
273 Ni and Co abundances measured in metal grains present within the matrices of these meteorites
274 (Fig. 5). Such a trend was also found in other unheated CMs and the ungrouped chondrite Acfer
275 094 (Kimura et al., 2008).

276 Troilite, pyrrhotite, and pentlandite were observed in these three chondrites. Pyrrhotite and
277 pentlandite contain 0.2-2.9 wt.% Ni and <0.3 wt.% Co, and 16-34 wt.% and 0.3-1.4 wt.%,
278 respectively.

279

280 3.3 Matrix

281 Table 3 and Fig. 6 show the average compositions of matrices in the three chondrites. These
282 compositions overlap with those in CMs, COs, and Acfer 094. They plot along the serpentine line,
283 which might indicate that serpentine is the major component of the matrices. However, the
284 average totals of the matrices by EPMA are 90-96 wt.%. These totals are higher than those of
285 phyllosilicates. Such high totals have previously been reported in the CM NWA 11024 that
286 experienced secondary heating (Ebert et al., 2019). In contrast to NWA 11024 there is little
287 evidence for heating of the three Asuka samples. The average apparent S weight percent in the
288 matrices of the Asuka samples is 4-5 wt.%. Such high S contents are consistent with abundant
289 sulfide grains of submicron size in the matrices.

290

291 3.4 X-ray diffraction

292 We measured the XRD patterns for the three Asuka CM chondrites. No phyllosilicates or
293 tochilinite were detected in A 12169 and A 12236 (Fig. 7a), in spite of the fact that rare or minor
294 phyllosilicates are present within their chondrules. Only A 12085 contains a small amount of
295 cronstedtite ($2\theta=12.3^\circ$) and tochilinite ($2\theta=16.4^\circ$). From the high modal abundance of the matrix,
296 we suggest that phyllosilicate and tochilinite are mainly present in the matrix of A 12085, although
297 phyllosilicate does also occur in the chondrules of A 12085. These relationships suggest that the
298 degree of alteration of A 12085 is somewhat higher than that of the other two chondrites. No

299 detection of phyllosilicate in A 12169 and A 12236 by the XRD indicates that their matrices are
300 mainly comprised of anhydrous minerals or amorphous phases. Since typical TCI is not observed
301 in A 12085, the occurrence of tochilinite is not yet evident. We need to undertake a further TEM
302 study to clarify this.

303 Olivine and clinoenstatite were identified by their XRD patterns (Figs. 7a and 7b). Figure 7b
304 shows that fayalitic olivine is encountered only in A 12169. The peak position, 31.9° , indicates
305 $\sim\text{Fa}_{50}$ olivine after the method by Imae and Nakamuta (2018). A small amount of orthoenstatite is
306 also seen in these chondrites. Kamacite, taenite, and troilite were commonly identified in the three
307 chondrites (Fig. 7c). Pyrrhotite was not detected by the XRD, although minor pyrrhotite is
308 identified by EPMA analysis. The major sulfide in these chondrites is troilite. Howard et al. (2009)
309 identified magnetite in CMs by the XRD technique. However, this phase was not identified in
310 these three chondrites, although rare magnetite was observed by FESEM as mentioned above.

311

312 3.5 Raman spectroscopy

313 The degree of heating experienced by the meteorites was evaluated using Raman
314 spectroscopy of matrix grains. For unequilibrated ordinary chondrites (UOC), the full-width at
315 half-maximum (FWHM) of the D-band decreases with increasing heating temperature, and the
316 intensity ratio I_D/I_G increases (Quirico et al. 2003). This constraint has been successfully applied to
317 type 2 and type 3 carbonaceous chondrites (Bonal et al. 2006; Bonal et al., 2007; Quirico et al.
318 2014).

319 The matrix Raman spectra from the three chondrites in this study exhibit first-order carbon D-
320 and G-bands at $\sim 1350\text{ cm}^{-1}$, and $\sim 1600\text{ cm}^{-1}$, respectively. Average I_D/I_G ratios are 0.836, 0.848,
321 0.841, and 0.931, and FWHM-D are 351.6 , 355.8 , 343.8 , and 269.1 cm^{-1} , for A 12085, A 12169, A

322 12236, and Murchison, respectively. These data are plotted in Fig. 8. All of the Asuka samples
323 show broad FWHM-D and low I_D/I_G , and plot within the area of primitive CR chondrites
324 (Komatsu et al., 2018). The matrix Raman characteristics of these three samples are distinguished
325 from other CMs, including Murchison (subtype 2.5), heated CMs, and COs and CVs of higher
326 petrologic types, indicating that they experienced very little heating.

327 We also measured some additional phases in these chondrites. Some mesostasis phases are
328 plagioclase with distinct peaks at 505 cm^{-1} , and 487 cm^{-1} , and glass with a broad peak at $\sim 500\text{ cm}^{-1}$.
329 We also identified calcite with a distinct peak at 1089 cm^{-1} .

330

331 3.6 Bulk compositions

332 Table 5 shows the bulk chemical composition of A 12236. Figure 9a shows Al/Mn versus
333 (Zn/Mn)x100 ratios of the samples. A 12236 plots within the area of CMs. Figure 9b shows the
334 CI-normalized bulk composition of A 12236, compared with those of Paris (CM2.7), Murchison
335 (CM2.5), Nogoya (CM2.2), NWA 11024 (dehydrated CM), and CM-mean. A 12236 has a quite
336 similar composition to those of other CMs, from refractory to volatile elements, except for a small
337 depletion of Na and Pb. NWA 11024 experienced significant terrestrial weathering and is enriched
338 in some elements, such as Li, K, and Pb. This enrichment is not apparent in A 12236 and other
339 CMs. It is clear that A 12236 has bulk chemical composition typical of CMs.

340

341 3.7 Oxygen isotopes

342 The three Asuka CMs analyzed in this study have the following oxygen isotope compositions:
343 A 12169: $\delta^{17}\text{O}$ -4.07 ‰; $\delta^{18}\text{O}$ 1.32 ‰; $\Delta^{17}\text{O}$ -4.75 ‰; A 12085: $\delta^{17}\text{O}$ -4.83 ‰; $\delta^{18}\text{O}$ -0.31 ‰; $\Delta^{17}\text{O}$
344 -4.67 ‰; A 12236: $\delta^{17}\text{O}$ -4.33 ‰; $\delta^{18}\text{O}$ 0.80 ‰; $\Delta^{17}\text{O}$ -4.75 ‰. These analyses are shown in Fig.

345 10 in relation to analyses of CM2, CO3 and anomalous C2 chondrites taken from the literature
346 (full references to data sources are given in the caption to Fig. 10). The three Asuka CMs plot away
347 from the field of “normal” CM2 chondrites (Clayton and Mayeda, 1999; Haack et al., 2012;
348 Hewins et al., 2014) and close to the field of CO3 falls (Alexander et al., 2018). The gap between
349 the COs and CMs, where the Asuka CMs plot, is occupied by a range of C2 and anomalous CM
350 chondrites (Greenwood et al., 2019; Lee et al., 2019). A number of these isotopically anomalous
351 CM-like meteorites, such as LEW 85311 (Lee et al., 2019) and NWA 5958 show many
352 mineralogical and petrological features typical of CMs, but like the Asuka CMs described here,
353 have experienced only limited degrees of aqueous alteration. It therefore seems likely that the CM
354 group extends from almost pristine examples that plot close to the CO3 field in Fig. 10, to highly
355 aqueous altered examples that have isotopically heavy oxygen isotope compositions (top right
356 corner of Fig. 10). EET 96029 (Lee et al., 2016) provides additional evidence in support of this
357 relationship, containing areas which are both minimally altered (EET 96029 AK) and other areas
358 which are heavily altered (EET 96029 OU). A linear regression line through the anomalous C2
359 samples in Fig. 10 ($y = -4.17 + 0.67x$ $R^2 = 0.95$) passes through the “normal” CM2 field. These
360 relationships are consistent with the CM parent body having experienced highly variable levels of
361 aqueous alteration. In addition, the fact that mildly altered samples, such as the Asuka CMs and
362 NWA 5958, plot close to the CO3 field, and in the case of LEW 85311 actually plots within it,
363 supports the original suggestion of Clayton and Mayeda (1999) that the anhydrous CM precursor
364 material was CO-like, at least in terms of its oxygen isotope composition.

365

366 4. Discussion

367 4.1 Classification of chemical group

368 At first, we discuss the chemical group classification of these Asuka chondrites in comparison
369 with the other C chondrites. They have characteristic features as follows; 1) The modal
370 abundances of chondrule and matrix (Table 1) are similar to those in CMs (Weisberg et al., 2006).
371 The especially high abundance of matrix characterizes CM chondrites. 2) Chondrule size
372 distribution (Table 2) resembles that of CMs (Weisberg et al., 2006). 3) Refractory inclusions are
373 commonly encountered, and their abundances are within the range of CMs (Table 1). 4) Fe-Ni
374 metal is present, although it is more abundant than typical CMs (Table 1). 5) The Fe-Mn
375 distribution in olivines in the Asuka samples is also consistent with that of “normal” CMs (Fig. 3a),
376 although COs have a similar trend (Schrader and Davidson, 2017). 6) Porphyritic and type I
377 chondrules are highly abundant (Table 2), which is also the case for CMs (Jones, 2012). 7) The
378 bulk composition of A 12236 is close to those of other CMs (Fig. 9a and 9b).

379 These features distinguish these three chondrites from those of other major C chondrite
380 groups such as COs and CVs, and ungrouped C chondrites, such as Acfer 094 (Newton et al.,
381 1995) and Y-82094 (Kimura et al., 2014). A 12085, A 12169, and A 12236 are, therefore,
382 classified as belonging to the CM group. This classification is further supported by the abundances
383 and isotopic compositions of H, C, and N in A 12236 by Nittler et al. (2020).

384

385 4.2 Primitive natures and secondary processes

386 4.2.1 Aqueous alteration

387 Rubin et al. (2007) and Rubin (2015) suggested that CMs are classified into subtypes 2.7-2.0,
388 based on many petrologic criteria that reflect the alteration degree. Here we discuss the alteration
389 degree of the Asuka CMs studied here on the basis of the subtype criteria.

390 Chondrule mesostasis: The mesostases in chondrules of subtype 2.7-2.0 are replaced by
391 phyllosilicates (Rubin, 2007). The chondrules in the Asuka CMs also contain phyllosilicates, with
392 the abundances increasing from A 12169 through A 12236 to A 12085. In most chondrules of A
393 12169, phyllosilicate, if it present, replaces the primary mesostasis only in the peripheries. On the
394 other hand, primary mesostasis phases (feldspar and glass) are abundant, not only in A 12169, but
395 also in A 12236 and A 12085. All these results suggest low degrees of alteration, lower than in
396 subtype 2.7.

397 Matrix phyllosilicates: CMs of subtypes 2.7-2.0 contain abundant phyllosilicates in their
398 matrices. Phyllosilicates were identified only in the matrix of A 12085 by XRD. In A 12169 and A
399 12236, phyllosilicate were not detected in the matrices by XRD. Noguchi et al. (2020) observed no
400 phyllosilicates in the matrix of A 12169 in TEM observations. These results indicate a lower
401 degree of alteration for A 12169 and A 12236 than in those of subtypes 2.7-2.0.

402 Matrix compositions: The matrix compositions, MgO/FeO and S/SiO₂ weight ratios, can be
403 used to classify the subtypes and increase and decrease with decreasing subtypes, respectively
404 (Rubin et al., 2007). The MgO/FeO and S/SiO₂ ratios are 0.59 and 0.14, 0.51 and 0.12, and 0.56
405 and 0.16, in A 12169, A 12236, and A 12085, respectively. These values overlap with or are higher
406 than those in subtypes 2.7-2.0 (0.35-0.7 for MgO/FeO and 0.05-0.18 for S/SiO₂).

407 Abundance of metal: The metal abundances in CMs decrease with decreasing subtype. The
408 modal abundances of Fe-Ni metal in the Asuka CMs are 1.2-2.3 vol.%, which are similar to or
409 higher than those in even subtype 2.7 (<2 vol.%). In particular, metal (2.3 vol.%) is much more
410 abundant in A 12169 than any known CM.

411 Phenocrysts in chondrules: Alteration features in phenocryst are common in subtypes 2.3-2.0.
412 On the other hand, all chondrules in the Asuka CMs have no any altered phenocrysts.

413 TCI: The abundance and occurrence of TCI and its composition are also criteria for the
414 classification into subtypes. However, the Asuka CMs do not contain typical TCI. Tsuchiyama et
415 al. (2020) reported possible precursors of TCI, Fe-rich hydrous silicate objects, in the matrix of A
416 12169 by TEM observation. Although fine-grained aggregates of sulfide and anhydrous silicates
417 are observed, especially in A 12085, they are not TCI.

418 Sulfide: Pyrrhotite and pentlandite in CMs and CRs are proposed to be primary sulfide phases
419 that originated under high-temperature conditions (Schrader et al., 2016; Singerling and Brearley,
420 2018). A 12169 contains such an assemblage (Fig. 2i), and they may represent high-temperature
421 products. On the other hand, the abundances of pentlandite and pyrrhotite are also the criteria for
422 the subtypes, and pentlandite increases with decreasing subtype (Rubin et al., 2007). The major
423 sulfide is troilite in the Asuka CMs. On the other hand, troilite hardly remains in the other CMs,
424 except in heated CMs (Nakamura, 2005).

425 Carbonate: Carbonate and its composition characterize the alteration degree. Ca-carbonate is
426 encountered in subtypes 2.7-2.0. However, it is rarely encountered in these chondrites. Chondrules
427 in A 12085 do contain some Ca-carbonate, whereas a tiny grain of Ca-carbonate occurs only in a
428 clast in A 12169.

429 Thus, most of these criteria for subtypes 2.7-2.0 cannot be applied to the classification of A
430 12085, A 12169, and A 12236. Instead, many characteristic features of these chondrites indicate
431 lower degrees of aqueous alteration for these chondrites, suggesting higher subtypes than 2.7. We
432 will discuss the subtypes for the Asuka CMs in a later section. The common occurrence of
433 unaltered melilite, especially in A 12169, provides additional support for these chondrites having
434 experienced very limited degrees of aqueous alteration, because melilite is easily altered by
435 secondary processes (Greenwood et al., 1994; Russell et al., 1998; Rubin, 1998). The degree of

436 alteration increases from A 12169, through A 12236, to A 12085. From the occurrence of
437 phyllosilicate and carbonate, the degree of aqueous alteration is higher for A 12085 than A 12236
438 and lower than for a CM2.7 such as Paris and others which abundantly contains phyllosilicate and
439 TCI (Hewins et al., 2014; Rubin 2007).

440

441 4.2.2 Secondary heating

442 Many CM or CM-related chondrites experienced heating (dehydration) after the aqueous
443 alteration. Nakamura (2005) and Kimura et al. (2011) proposed the classification criteria for the
444 degree of heating, such as decomposition of phyllosilicates and sulfide texture. A wide variety of
445 silicate compositions indicate that these chondrites did not experience significant prolonged
446 heating. From mineralogy, A 12085, A 12169, and A 12236 belong to stage I of Nakamura (2005),
447 suggesting that they did not experience heating higher than 250 °C. This is supported by the
448 occurrence of glass and clinoenstatite in chondrules, and the lack of ferroan rims on AOA olivines.
449 Feldspar does not show devitrification texture with high-Ca pyroxene. Such an occurrence
450 supports that proposition that little or no heating took place.

451 Rare plessitic features, a positive correlation between Ni and Co, and the compositional
452 distribution of Si, P, and Cr in Fe-Ni metal are only observed in very primitive chondrites, such as
453 Acfer 094 that did not experience secondary heating (Kimura et al., 2008 and 2011). The Asuka
454 CMs have all these features in their Fe-Ni metal.

455 In heated CMs, pyrrhotite commonly has pentlandite blebs or lamella. On the other hand, such
456 blebs and lamella in pyrrhotite are rare in unheated CMs (Category A after Kimura et al., 2011).
457 The Asuka CMs show similar features to unheated CMs (Kimura et al., 2011). Therefore, the
458 Asuka CMs are classified as Category A.

459 The Raman spectral features of the matrices also indicate low degrees of heating. The Asuka
460 CMs plot within the range of unheated CR chondrites (Komatsu et al., 2018), and are distinct from
461 those of heated CMs, and metamorphosed CO, CV, and ordinary chondrites (Fig. 8). The matrices
462 of the Asuka CMs contain abundant S due to the presence of submicron sulfide grains. Abundant
463 and finely disseminated S in matrix is a feature of other primitive (almost unheated) chondrites
464 (e.g., Grossman and Brearley, 2005).

465 We conclude that the Asuka CMs did not experienced any heating. Therefore, we suggest that
466 the absence or rare occurrence of phyllosilicates and TCIs in the Asuka CMs are not the result of
467 thermal decomposition, but rather reflect the very limited aqueous alteration that these chondrites
468 have experienced.

469

470 4.2.3 Pristine CMs

471 Recently some CM or CM-related chondrites have been reported to have mineralogies
472 consistent with having experienced relatively low degrees of aqueous alteration, as mentioned
473 before. However, Paris, EET 96029, and LEW 85311 are classified as CM2.7, and still contain
474 abundant phyllosilicates (Hewins et al., 2014; Lee et al., 2016; Lee et al., 2019). CM-related NWA
475 5958 contains phyllosilicate and TCI. NWA 11024 is classified as type 3, but it experienced
476 secondary dehydration after weak aqueous alteration. All these chondrites seem to show higher
477 degrees of alteration than A 12169 and others. Therefore, these Asuka chondrites studied here,
478 especially A 12169, are the most primitive CM so far reported.

479 Noguchi et al. (2020) found predominant amorphous materials with enstatite whisker and no
480 phyllosilicate in the matrix of A 12169 in a TEM study. They suggested that the alteration degree
481 of A 12169 is lower than Paris. Nittler et al. (2020) suggested that A 12236 is the most pristine CM

482 from the isotopic compositions and abundance of H, C, and N, and abundant presolar grains. All
483 these results are consistent with our conclusions.

484

485 4.3 Classification of petrologic type

486 All CM chondrites were originally classified as petrologic type 2 (Van Schmus and Wood,
487 1967). Later many different criteria were proposed to classify varying degrees of alteration that
488 were experienced by the CMs, such as the matrix features (McSween, 1979), mineralogical index
489 (Browning et al., 1996), petrological features (Rubin et al., 2007), the analysis of H, C, and N
490 (Alexander et al., 2013), and phyllosilicate fraction (Howard et al., 2015). Among them, the
491 scheme of Rubin et al. (2007) is widely used as it provides a relatively straightforward means of
492 classifying the CMs and accordingly we use it here to assign the Asuka CMs to their appropriate
493 subtypes.

494 Rubin et al. (2007) and Rubin (2015) proposed subtypes for CMs that were not heated. Since
495 the Asuka CMs studied here are not only unheated, but also unbrecciated, they are suitable
496 samples for the application of the Rubin et al. (2007) and Rubin (2015) schemes. The Asuka CMs
497 should be assigned subtypes that are higher than 2.7 as discussed above. Rubin et al. (2007)
498 hypothesized that CM3.0 samples would have some distinct features that would help to identify
499 them, such as the occurrence of chondrule glass and minor phyllosilicate. Based on the results of
500 our study of the Asuka CMs, we have modified the scheme of Rubin et al. (2007) and propose the
501 following criteria for CM3.0 to 2.8 (Table 6).

502 CM3.0: The most distinguishing feature of this subtype is the abundant primary glass and
503 feldspar in chondrule mesostasis. Phenocrysts in chondrules do not show any alteration features.
504 Phyllosilicates are rarely encountered in chondrules. A small amount of phyllosilicate is also

505 observed in other primitive chondrites, such as ALH 77307 (CO3.03). However, no chondrules
506 with completely altered mesostasis were observed. The matrix has no phyllosilicate, and the
507 compositions, MgO/FeO and S/SiO₂ ratios are >0.5 and >0.1, respectively. TCI and carbonate are
508 absent in them. Although the A 12169 section contain tiny Ca-carbonate, it is only in a clast. Fe-Ni
509 metal is abundant, >2 vol.%, in chondrules and matrix. The major sulfide is troilite, although
510 minor pyrrhotite-pentlandite is present. Harju et al. (2014) proposed the criteria for hypothetical
511 “CR3”, such as abundant glass in chondrules, no phenocryst alteration, and no phyllosilicate in the
512 matrix. These criteria are nearly the same as those for CM3.0 presented here.

513 CM2.9: The primary mesostasis abundantly survives in chondrules. However, about half of
514 the chondrules have partly to completely altered mesostasis. Phyllosilicates are not detected by the
515 XRD because of their minor abundance. No occurrence of TCI and carbonate, and the abundance
516 of troilite is nearly the same as subtype 3.0, although the metal abundance is 1-2 vol. %.

517 CM 2.8: In chondrules, phyllosilicate is more abundant than primary mesostasis, although
518 phenocrysts are not yet altered. Only a minor amount of phyllosilicate is present, mainly in the
519 matrix. Tochilinite is also detected by the XRD, although typical TCI is not observed. The metal
520 abundance is nearly the same as CM2.9. Troilite is still the major sulfide mineral. Carbonate may
521 be present.

522 From these criteria, A 12169, A 12236, and A 12085 are classified as subtype 3.0, 2.9, and 2.8,
523 respectively. Although the three Asuka CMs have similar features such as petrography and oxygen
524 isotopic compositions, the alteration degrees (subtypes) are evidently different and they were
525 recovered from the wide area, as mentioned above. Therefore, it is an open question as whether
526 these samples are paired and we cannot totally exclude the possibility that they represent different
527 lithologies from the same breccia.

528

529 4.4 Primitive features of CM chondrites

530 Most CMs so far described experienced some combination of aqueous alteration, heating, and
531 brecciation, and have lost many of their primary features. On the other hand, the Asuka CMs, in
532 particular A 12169 CM3.0, hardly experienced these secondary processes. The terrestrial
533 weathering degrees also low. Therefore, these chondrites provide a unique opportunity to explore
534 the primary features of CM chondrites, as well as potential genetic relationships amongst the
535 CM-CO clan chondrites.

536 From the characteristic features of the Asuka CMs, we infer that unmodified chondrules and
537 refractory inclusions in CMs have many features that are common to all C chondrite groups, such
538 as abundant porphyritic chondrules with unaltered phenocrysts that are predominantly type I, pure
539 forsteritic olivine in AOAs, melilite-bearing CAIs, and the occurrence of Fe-Ni metal and troilite.
540 Primary matrix materials consisted of anhydrous minerals or amorphous phases. Amorphous
541 materials have also been reported in the matrices of some primitive CMs and COs (e.g., Brearley,
542 1993; Leroux et al. 2015; Davidson et al. 2019). Fayalitic olivine ($\sim\text{Fa}_{50}$) was only detected in A
543 12169 by XRD, although Noguchi et al. (2020) also reported similar olivine from the matrix of A
544 12169 in TEM study. Such ferroan olivine was also discovered in the matrices of other primitive C
545 chondrites (e.g., Brearley, 1993; Scott and Krot, 2006). All these primary features were partly to
546 completely lost from most CMs during aqueous alteration.

547 The CMs, including the Asuka CMs, have lower abundances of refractory inclusions and
548 opaque minerals but higher abundances of matrix when compared to all other types of C
549 chondrites. These features should be unique original features of CMs from the stage of precursor
550 materials. A 12236 (CM2.9), Paris (CM2.7), Murchison (2.5), and Nogoya (2.2) have quite similar

551 bulk compositions to each other, in spite of the wide variation in degree of aqueous alteration. This
552 suggests that the bulk chemistry was not changed during aqueous alteration, as suggested by Rubin
553 et al. (2007).

554 Kallemeyn and Wasson (1982) proposed that the CM and CO chondrites shared the same
555 parent body and constituted a CM-CO clan. However, since CMs were aqueously altered unlike
556 the COs, it has been difficult to compare the precursor materials to both groups. However, we can
557 suggest that the primary materials of the CMs and COs were different from one another, especially
558 chondrule size, the abundances of matrix, inclusions, and opaque minerals, and bulk compositions,
559 as also suggested by Schrader and Davidson (2017) and Chaumard et al. (2018). Although the
560 CMs and COs had anhydrous minerals with similar oxygen isotopic compositions (Kallemeyn and
561 Wasson, 1982), COs contained the smaller chondrules and lower abundances of the matrix and
562 refractory inclusions than primitive CMs. Therefore, we suggest that CMs and COs were derived
563 from different parent bodies. Later, COs experienced very mild aqueous alteration and varying
564 degrees of thermal metamorphism (e.g., Sears et al., 1991). On the other hand, most CMs were
565 weakly to heavily subjected to aqueous alteration. Later some CMs experienced varying degrees
566 of heating in their parent body. The results obtained here indicate that the CM parent body
567 experienced very variable degrees of aqueous alteration.

568 While the CO and CM chondrites appear to show clear mineralogical and petrological
569 differences, from an oxygen isotope perspective, both groups exhibit clear affinities (Fig. 10). The
570 precursor material to the CMs, appears to have been isotopically nearly identical to that of the CO
571 falls. It appears likely that both groups originated from a similar mix of primary components, with
572 the likely distinction that CMs contained a higher content of volatile constituents (water ice?). This
573 suggests that the parent bodies to both groups may have accreted in a similar region of the nebula.

574 It has been suggested by Chaumard et al. (2018) that chondrules in COs and CMs may have
575 formed in the same disk location, but that the CO parent body accreted before that of the CM. They
576 suggested that between these two accretion events the snow line may have moved inwards, such
577 that the CO parent body formed without a significant water ice fraction, whereas the CM parent
578 body did. Our study of the Asuka CMs, particularly their oxygen isotope compositions, further
579 highlights the strong relationship between CMs and COs, while also indicating that they are
580 probably not both derived from a single heterogeneous parent body.

581

582 **5. Conclusions**

583 We studied three Asuka carbonaceous chondrites. They are CMs, based on their modal
584 compositions, chondrule size distributions, and bulk compositions. They experienced minimal to
585 weak secondary processes such as aqueous alteration and heating. The degree of alteration
586 increases from A 12169, through A 12236, to A 12085, and we propose that they are classified as
587 subtypes 3.0 to 2.8, respectively.

588 We suggest that these chondrites, especially A 12169, are the most primitive CMs so far
589 described. These new CMs provide a unique opportunity to investigate the primary features of
590 CMs, as well as the genetic relationships of CM-CO clan chondrites. While showing strong
591 affinities in terms of their oxygen isotope compositions, CMs and COs were probably derived
592 from different parent bodies.

593 The CMs experienced complicated parent body processes. However, the classification
594 scheme proposed here is useful, not only for classification purposes, but the exploration of the
595 precursor materials and the history and evolution of the CM parent body.

596 The asteroids Ryugu and Bennu are related to hydrated chondrites, especially CMs (e.g.,
597 Hamilton et al., 2019; Morota et al., 2020), although Ryugu may have experienced heating by the
598 Sun. On the other hand, the Asuka CMs studied here hardly experienced hydration and heating.
599 However, as breccias are common in CM chondrites (Metzler et al., 1992) and the surface
600 materials of the Ryugu and Bennu are highly variable, we expect that returned samples may
601 contain some of the least altered materials, comparable to the Asuka CMs. Therefore, these
602 chondrites are also of particular significance in view of the imminent return of sample material
603 from the asteroids Ryugu and Bennu.

604

605

606 **Acknowledgements**

607 The sections were loaned from the National Institute of Polar Research. One of Murchison
608 sections was loaned from T. Fagan. We appreciate the thoughtful reviews by two anonymous
609 reviewers. We also thank the associate editor Kevin Righter for efficient handling of the
610 manuscript. This work was supported by a Grant-in-aids of Ministry of Education, Science, Sport,
611 and Culture of Japanese government, No. 18K03729 to M. K. This study was also supported by
612 National Institute of Polar Research (NIPR) through Project research KP307 and General
613 Collaboration Project no. 30-21. Oxygen isotope studies at the Open University are funded by a
614 consolidated grant from the Science and Technology Facilities Council (STFC), UK GRANT
615 NUMBER: ST/P000657/1.

616

617 **References**

- 618 Alexander, C.M.O.D., Howard, K.T., Bowden, R., Fogel, M.L., 2013. The classification of CM
619 and CR chondrites using bulk H, C and N abundances and isotopic compositions.
620 *Geochimica et Cosmochimica Acta.* 123, 244-260.
- 621 Alexander C. M. O'D., Greenwood R. C., Bowden R., Gibson J. M., Howard K. T. and Franchi I.
622 A. (2018) A multi-technique search for the most primitive CO chondrites. *Geochim.*
623 *Cosmochim. Acta* 221, 406-420.
- 624 Anders, E., Grevesse, N., 1989. Abundances of the elements: Meteoritic and solar. *Geochimica et*
625 *Cosmochimica Acta.* 53, 197-214.
- 626 Barrat, J.A., Zanda, B., Moynier, F., Bollinger, C., Liorzou, C., Bayon, G., 2012. Geochemistry of
627 CI chondrites: Major and trace elements, and Cu and Zn Isotopes. *Geochimica et*
628 *Cosmochimica Acta.* 83, 79-92.
- 629 Bonal L, Quirico E, Bourot-Denise M, Montagnac G., 2006. Determination of the petrologic type of CV3
630 chondrites by Raman spectroscopy of included organic matter. *Geochimica et Cosmochimica Acta*
631 70, 1849-1863.
- 632 Bonal L, Bourot-Denise M, Quirico E, Montagnac G, Lewin E., 2007. Organic matter and metamorphic
633 history of CO chondrites. *Geochimica et Cosmochimica Acta* 71, 1605-1623. Brearley, A.J., 1993.
634 Matrix and fine-grained rims in the unequilibrated CO3 chondrite, ALHA77307: Origins and
635 evidence for diverse, primitive nebular dust components. *Geochimica et Cosmochimica Acta.* 57,
636 1521-1550.
- 637 Braukmüller, N., Wombacher, F., Hezel, D.C., Escoube, R., Münker, C., 2018. The chemical composition
638 of carbonaceous chondrites: Implications for volatile element depletion, complementarity and
639 alteration. *Geochimica et Cosmochimica Acta.* 239, 17-48.

- 640 Browning, L.B., McSween, H.Y.J., Zolensky, M.E., 1996. Correlated alteration effects in CM
641 carbonaceous chondrites. *Geochimica et Cosmochimica Acta*. 60, 2621-2633.
- 642 Busemann, H., Alexander, C.M.O'D., Nittler, L., R., 2007. Characterization of insoluble organic matter in
643 primitive meteorites by microRaman spectroscopy. *Meteoritics & Planetary Sciences*. 42,
644 1387-1416.
- 645 Chaumard, N., Defouilloy, C., Kita, N.T., 2018. Oxygen isotope systematics of chondrules in the
646 Murchison CM2 chondrite and implications for the CO-CM relationship. *Geochimica et*
647 *Cosmochimica Acta*. 228, 220-242.
- 648 Clayton, R.N., Mayeda, T.K., 1984. The oxygen isotope record in Murchison and other carbonaceous
649 chondrites. *Earth and Planetary Science Letters*. 67, 151-161.
- 650 Clayton R. N. and Mayeda T. K. (1999) Oxygen isotope studies of carbonaceous chondrites. *Geochim.*
651 *Cosmochim. Acta* 63, 2089–2104.
- 652 Davidson, J., Alexander, C.M.O.D., Stroud, R.M., Busemann, H., Nittler, L.R., 2019. Mineralogy and
653 petrology of Dominion Range 08006: A very primitive CO₃ carbonaceous chondrite. *Geochimica*
654 *et Cosmochimica Acta*. 265, 259-278.
- 655 Ebert, S., Patzek, M., Lentfort, S., Bischoff, A., 2019. Accretion of differentiated achondritic and
656 aqueously altered chondritic materials in the early solar system—Significance of an igneous
657 fragment in the CM chondrite NWA 12651. *Meteoritics & Planetary Science*. 54,
658 2985-2995.
- 659 Greenwood, R.C., Lee, M.R., Hutchison, R., Barber, D.J., 1994. Formation and alteration of CAIs
660 in Cold Bokkeveld (CM2). *Geochimica et Cosmochimica Acta*. 58, 1913-1935.

- 661 Greenwood, R.C., Franchi, I.A., Gibson, J.M., Benedix, G.K., 2012. Oxygen isotope variation in
662 primitive achondrites: The influence of primordial, asteroidal and terrestrial processes.
663 *Geochimica et Cosmochimica Acta*. 94, 146-163.
- 664 Greenwood R. C., Burbine T. H., Miller M. F., and Franchi I. A. 2017 Melting and differentiation
665 of early-formed asteroids: The perspective from high precision oxygen isotope studies:
666 *Chemie der Erde-Geochemistry* 77, 1-43.
- 667 Greenwood, R.C., Howard, K.T., King, A.J., Lee, M.R., Burbine, T.H., Franchi, I.A., Anand, M.,
668 Findlay, R., Gibson, J.M. A. 2019. Oxygen isotope evidence for multiple CM parent bodies:
669 What will we learn from the Hayabusa2 and OSIRIS-Rex sample return mission? (abstract).
670 *Lunar and Planetary Science*. 50, 2132.
- 671 Grossman, J.N., Brearley, A.J., 2005. The onset of metamorphism in ordinary and carbonaceous
672 chondrites. *Meteoritics & Planetary Science*. 40, 87-122.
- 673 Haack, H., Grau, T., Bischoff, A., Horstmann, M., Wasson, J., Sørensen, A., Laubenstein, M., Ott,
674 U., Palme, H., Gellissen, M., Greenwood, R., Pearson, V. K., Franchi, I. A., Gabelica, Z.,
675 Schmitt-Kopplin, P., 2012 Maribo—A new CM fall from Denmark. *Meteoritics & Planetary
676 Science*, 47, 30-50.
- 677 Hamilton, V.E., Simon, A.A., Christensen, P.R., Reuter, D.C., Clark, B.E., Barucci, M.A., Bowles,
678 N.E., Boynton, W.V., Brucato, J.R., Cloutis, E.A., Connolly, H.C., Donaldson Hanna, K.L.,
679 Emery, J.P., Enos, H.L., Fornasier, S., Haberle, C.W., Hanna, R.D., Howell, E.S., Kaplan,
680 H.H., Keller, L.P., Lantz, C., Li, J.Y., Lim, L.F., McCoy, T.J., Merlin, F., Nolan, M.C., Praet,
681 A., Rozitis, B., Sandford, S.A., Schrader, D.L., Thomas, C.A., Zou, X.D., Lauretta, D.S.,
682 Highsmith, D.E., Small, J., Vokrouhlický, D., Bowles, N.E., Brown, E., Donaldson Hanna,
683 K.L., Warren, T., Brunet, C., Chicoine, R.A., Desjardins, S., Gaudreau, D., Haltigin, T.,

684 Millington-Veloza, S., Rubi, A., Aponte, J., Gorius, N., Lunsford, A., Allen, B., Grindlay, J.,
685 Guevel, D., Hoak, D., Hong, J., Schrader, D.L., Bayron, J., Golubov, O., Sánchez, P.,
686 Stromberg, J., Hirabayashi, M., Hartzell, C.M., Oliver, S., Rascon, M., Harch, A., Joseph, J.,
687 Squyres, S., Richardson, D., Emery, J.P., McGraw, L., Ghent, R., Binzel, R.P., Asad,
688 M.M.A., Johnson, C.L., Philpott, L., Susorney, H.C.M., Cloutis, E.A., Hanna, R.D.,
689 Connolly, H.C., Ciceri, F., Hildebrand, A.R., Ibrahim, E.M., Breitenfeld, L., Glotch, T.,
690 Rogers, A.D., Clark, B.E., Ferrone, S., Thomas, C.A., Campins, H., Fernandez, Y., Chang,
691 W., Chevront, A., Trang, D., Tachibana, S., Yurimoto, H., Brucato, J.R., Poggiali, G.,
692 Pajola, M., Dotto, E., Mazzotta Epifani, E., Crombie, M.K., Lantz, C., Izawa, M.R.M., de
693 Leon, J., Licandro, J., Garcia, J.L.R., Clemett, S., Thomas-Keprta, K., Van wal, S.,
694 Yoshikawa, M., Bellerose, J., Bhaskaran, S., Boyles, C., Chesley, S.R., Elder, C.M.,
695 Farnocchia, D., Harbison, A., Kennedy, B., Knight, A., Martinez-Vlasoff, N., Mastrodemos,
696 N., McElrath, T., Owen, W., Park, R., Rush, B., Swanson, L., Takahashi, Y., Velez, D.,
697 Yetter, K., Thayer, C., Adam, C., Antreasian, P., Bauman, J., Bryan, C., Carcich, B., Corvin,
698 M., Geeraert, J., Hoffman, J., Leonard, J.M., Lessac-Chenen, E., Levine, A., McAdams, J.,
699 McCarthy, L., Nelson, D., Page, B., Pelgrift, J., Sahr, E., Stakkestad, K., Stanbridge, D.,
700 Wibben, D., Williams, B., Williams, K., Wolff, P., Hayne, P., Kubitschek, D., Barucci, M.A.,
701 Deshapriya, J.D.P., Fornasier, S., Fulchignoni, M., Hasselmann, P., Merlin, F., Praet, A.,
702 Bierhaus, E.B., Billett, O., Boggs, A., Buck, B., Carlson-Kelly, S., Cerna, J., Chaffin, K.,
703 Church, E., Coltrin, M., Daly, J., Deguzman, A., Dubisher, R., Eckart, D., Ellis, D.,
704 Falkenstern, P., Fisher, A., Fisher, M.E., Fleming, P., Fortney, K., Francis, S., Freund, S.,
705 Gonzales, S., Haas, P., Hasten, A., Hauf, D., Hilbert, A., Howell, D., Jaen, F., Jayakody, N.,
706 Jenkins, M., Johnson, K., Lefevre, M., Ma, H., Mario, C., Martin, K., May, C., McGee, M.,

- 707 Miller, B., Miller, C., Miller, G., Mirfakhrai, A., Muhle, E., Norman, C., Olds, R., Parish, C.,
708 Ryle, M., Schmitzer, M., Sherman, P., Skeen, M., Susak, M., Sutter, B., Tran, Q., Welch, C.,
709 Witherspoon, R., Wood, J., Zareski, J., Arvizu-Jakubicki, M., Asphaug, E., Audi, E.,
710 Ballouz, R.L., Bandrowski, R., Becker, K.J., Becker, T.L., Bendall, S., Bennett, C.A.,
711 Bloomenthal, H., Blum, D., Boynton, W.V., Brodbeck, J., Burke, K.N., Chojnacki, M.,
712 Colpo, A., Contreras, J., Cutts, J., Drouet d'Aubigny, C.Y., Dean, D., DellaGiustina, D.N.,
713 Diallo, B., Drinnon, D., Drozd, K., Enos, H.L., Enos, R., Fellows, C., Ferro, T., Fisher, M.R.,
714 Fitzgibbon, G., Fitzgibbon, M., Forelli, J., Forrester, T., Galinsky, I., Garcia, R., Gardner, A.,
715 Golish, D.R., Habib, N., Hamara, D., Hammond, D., Hanley, K., Harshman, K.,
716 Hergenrother, C.W., Herzog, K., Hill, D., Hoekenga, C., Hooven, S., Howell, E.S., Huettner,
717 E., Janakus, A., Jones, J., Kareta, T.R., Kidd, J., Kingsbury, K., Balram-Knutson, S.S.,
718 Koelbel, L., Kreiner, J., Lambert, D., Lauretta, D.S., Lewin, C., Lovelace, B., Loveridge, M.,
719 Lujan, M., Maleszewski, C.K., Malhotra, R., Marchese, K., McDonough, E., Mogk, N.,
720 Morrison, V., Morton, E., Munoz, R., Nelson, J., Nolan, M.C., Padilla, J., Pennington, R.,
721 Polit, A., Ramos, N., Reddy, V., Riehl, M., Rizk, B., Roper, H.L., the, O.-R.T., 2019.
722 Evidence for widespread hydrated minerals on asteroid (101955) Bennu. 2019. *Nature*
723 *Astronomy*. 3, 332-340.
- 724 Harju, E.R., Rubin, A.E., Ahn, I., Choi, B.-G., Ziegler, K., Wasson, J.T., 2014. Progressive
725 aqueous alteration of CR carbonaceous chondrites. *Geochimica et Cosmochimica Acta*. 139,
726 267-292.
- 727 Hewins, R.H., Bourot-Denise, M., Zanda, B., Leroux, J., Barrat, J.A., Humayun, M., Göpel, C.,
728 Greenwood, R.C., Franchi, I.A., Pont, S., Lorand, J.P., Cournède, C., Gattacceca, J.,

- 729 Rochette, P., Kuga, M., Marrocchi, Y., Marty, B., 2014. The Paris meteorite, the least altered
730 CM chondrite so far. *Geochimica et Cosmochimica Acta*. 124, 190-222.
- 731 Howard, K.T., Benedix, G.K., Bland, P.A., Cressey, G., 2009. Modal mineralogy of CM2
732 chondrites by X-ray diffraction (PSD-XRD). Part 1: Total phyllosilicate abundance and the
733 degree of aqueous alteration. *Geochimica et Cosmochimica Acta*. 73, 4576-4589.
- 734 Howard, K.T., Alexander, C.M.O.D., Schrader, D.L., Dyl, K.A., 2015. Classification of hydrous
735 meteorites (CR, CM and C2 ungrouped) by phyllosilicate fraction: PSD-XRD modal
736 mineralogy and planetesimal environments. *Geochimica et Cosmochimica Acta*. 149,
737 206-222.
- 738 Ikeda, Y., 1983. Alteration of chondrules and matrices in the four Antarctic carbonaceous
739 chondrites ALH-77307(C3), Y-790123(C2), Y-75293(C2), and Y-74662(C2). *Mem. Natl.*
740 *Inst. Polar Res. Spec. Issue* 30, 93-108.
- 741 Imae N., Debaille V., Akada Y., Debouge W., Goderis S., Hublet G., Mikouchi T., Van Roosbroek
742 N., Yamaguchi A., Zekollari H., Claeys P., Kojima H., 2015. Report of the JARE-54 and
743 BELARE 2012-2013 joint expedition to collect meteorites on the Nansen Ice Field,
744 Antarctica. *Antarctic Record* 59, 38-72.
- 745 Imae, N., Kimura, M., Yamaguchi, A., Kojima, H., 2019. Primordial, thermal, and shock features
746 of ordinary chondrites: Emulating bulk X-ray diffraction using in-plane rotation of polished
747 thin sections. *Meteoritics & Planetary Science*. 54, 919-937.
- 748 Imae, N., Nakamuta, Y., 2018. A new mineralogical approach for CO3 chondrite characterization
749 by X-ray diffraction: Identification of primordial phases and thermal history. *Meteoritics &*
750 *Planetary Science*. 53, 232-248.

- 751 Jacquet E., Barrat J-A., Beck P., Caste F., Gattacceca J., Sonzogni C. and Gounelle M. (2016).
752 Northwest Africa 5958: A weakly altered CM-related ungrouped chondrite, not a CI3.
753 Meteorit. Planet. Sci. 51, 851–869.
- 754 Jones, R.H., 2012. Petrographic constraints on the diversity of chondrule reservoirs in the
755 protoplanetary disk. Meteoritics & Planetary Science. 47, 1176-1190.
- 756 Kallemeyn, G.W., Wasson, J.T., 1981. The compositional classification of chondrites-I. The
757 carbonaceous chondrite groups. Geochimica et Cosmochimica Acta. 45, 1217-1230.
- 758 Kallemeyn, G.W., Wasson, J.T., 1982. The compositional classification of chondrites:III.
759 Ungrouped carbonaceous chondrites. Geochimica et Cosmochimica Acta. 46, 2217-2228.
- 760 Kallemeyn, G.W., Rubin, A.E., Wasson, J.T., 1994. The compositional classification of
761 chondrites: VI. The CR carbonaceous chondrite group. Geochimica et Cosmochimica Acta.
762 58, 2873-2888.
- 763 Kimura, M., Barrat, J.A., Weisberg, M.K., Imae, N., Yamaguchi, A., Kojima, H., 2014. Petrology
764 and bulk chemistry of Yamato-82094, a new type of carbonaceous chondrite. Meteoritics &
765 Planetary Science. 49, 346-357.
- 766 Kimura, M., Grossman, J.N., Weisberg, M.K., 2008. Fe-Ni metal in primitive chondrites:
767 Indicators of classification and metamorphic conditions for ordinary and CO chondrites.
768 Meteoritics and Planetary Science. 43, 1161-1177.
- 769 Kimura, M., Grossman, J.N., Weisberg, M.K., 2011. Fe-Ni metal and sulfide minerals in CM
770 chondrites: An indicator for thermal history. Meteoritics & Planetary Science 46, 431-442.
- 771 Kimura, M., Ikeda, Y., 1995. Anhydrous alteration of Allende chondrules in the solar nebula II:
772 Alkali-Ca exchange reactions and formation of nepheline, sodalite and Ca-rich phases in
773 chondrules. Proc. NIPR Symp. Antarc. Meteorites. 8, 123-138.

- 774 Kimura, M., Imae, N., Yamaguchi, A., Greenwood, R. C., Komatsu, M., Noguchi, T. 2019.
775 Primitive CM-related chondrites: their characteristic features and classification (abstract).
776 82nd Annual Meeting of the Meteoritical Society. #6042
- 777 Kimura, M., Mikouchi, T., Suzuki, A., Miyahara, M., Ohtani, E., El Goresy, A., 2009. Kushiroite,
778 CaAlAlSiO_6 : A new mineral of the pyroxene group from the ALH 85085 CH chondrite, and
779 its genetic significance in refractory inclusions. *American Mineralogist*. 94, 1479-1482.
- 780 Kimura, M., Yamaguchi, A., Miyahara, M., 2017. Shock-induced thermal history of an EH3
781 chondrite, Asuka 10164. *Meteoritics & Planetary Science*. 52, 24-35.
- 782 Komatsu, M., Fagan, T.J., Mikouchi, T., Petaev, M.I., Zolensky, M.E., 2015. LIME silicates in
783 amoeboid olivine aggregates in carbonaceous chondrites: Indicator of nebular and asteroidal
784 processes. *Meteoritics & Planetary Science*. 50, 1271-1294.
- 785 Komatsu, M. et al., 2018. First evidence for silica condensation within the solar protoplanetary
786 disk. *Proceedings of the National Academy of Sciences*. 115, 7497-7502.
- 787 Krot, A.N., Keil, K., Scott, E., R., D., Goodrich, C.A., Weisberg, M.K., 2014. Classification of
788 Meteorites and Their Genetic Relationships. In: Davis, A.M. (Ed.), *Treatise on Geochemistry*
789 1, Meteorites, Comets, and Planets 2nd Edition. Elsevier, Amsterdam, pp. 1-63.
- 790 Lee, M.R., Lindgren, P., 2016. Aqueous alteration of chondrules from the Murchison CM
791 carbonaceous chondrite: Replacement, pore filling, and the genesis of polyhedral serpentine.
792 *Meteoritics & Planetary Science*. 51, 1003-1021.
- 793 Lee, M.R., Lindgren, P., King, A.J., Greenwood, R.C., Franchi, I.A., Sparkes, R., 2016. Elephant
794 Moraine 96029, a very mildly aqueously altered and heated CM carbonaceous chondrite:
795 Implications for the drivers of parent body processing. *Geochimica et Cosmochimica Acta*.
796 187, 237-259.

- 797 Lee, M. R., Cohen, B. E., King, A. J., Greenwood, R. C., 2019. The diversity of CM carbonaceous
798 chondrite parent bodies explored using Lewis Cliff 85311. *Geochimica et Cosmochimica*
799 *Acta*, 264, 224-244.
- 800 Leroux, H., Libourel, G., Lemelle, L., Guyot, F., 2003. Experimental study and TEM
801 characterization of dusty olivines in chondrites: Evidence for formation by in-situ reduction.
802 *Meteoritics & Planetary Science*. 38, 81-94.
- 803 Leroux, H., Cuvillier, P., Zanda, B., Hewins, R.H., 2015. GEMS-like material in the matrix of the
804 Paris meteorite and the early stages of alteration of CM chondrites. *Geochimica et*
805 *Cosmochimica Acta*. 170, 247-265.
- 806 Lodders K. and Fegley B. Jr. 1998. *The planetary scientist's companion*. New York: Oxford
807 University Press. 371 p.
- 808 Marrocchi, Y., Gounelle, M., Blanchard, I., Caste, F., Kearsley, A.T., 2014. The Paris CM
809 chondrite: Secondary minerals and asteroidal processing. *Meteoritics & Planetary Science*.
810 49, 1232-1249.
- 811 McSween, H.Y., Jr., 1979. Alteration in CM carbonaceous chondrites inferred from modal and
812 chemical variations in matrix. *Geochimica et Cosmochimica Acta*. 43, 1761-1770.
- 813 Metzler, K., Bischoff, A., Stöffler, D., 1992. Accretionary dust mantles in CM chondrites:
814 Evidence for solar nebula processes. *Geochimica et Cosmochimica Acta*. 56, 2873-2897.
- 815 Miller, M.F., Franchi, I.A., Sexton, A.S., Pillinger, C.T., 1999. High precision $\Delta^{17}\text{O}$ isotope
816 measurements of oxygen from silicates and other oxides: Methods and applications. *Rapid*
817 *Comm. Mass Spec.* 13, 1211-1217.
- 818 Morota, T., Sugita, S., Cho, Y., Kanamaru, M., Tatsumi, E., Sakatani, N., Honda, R., Hirata, N.,
819 Kikuchi, H., Yamada, M., Yokota, Y., Kameda, S., Matsuoka, M., Sawada, H., Honda, C.,

- 820 Kouyama, T., Ogawa, K., Suzuki, H., Yoshioka, K., Hayakawa, M., Hirata, N., Hirabayashi,
821 M., Miyamoto, H., Michikami, T., Hiroi, T., Hemmi, R., Barnouin, O.S., Ernst, C.M.,
822 Kitazato, K., Nakamura, T., Riu, L., Senshu, H., Kobayashi, H., Sasaki, S., Komatsu, G.,
823 Tanabe, N., Fujii, Y., Irie, T., Suemitsu, M., Takaki, N., Sugimoto, C., Yumoto, K., Ishida,
824 M., Kato, H., Moroi, K., Domingue, D., Michel, P., Pilorget, C., Iwata, T., Abe, M., Ohtake,
825 M., Nakauchi, Y., Tsumura, K., Yabuta, H., Ishihara, Y., Noguchi, R., Matsumoto, K.,
826 Miura, A., Namiki, N., Tachibana, S., Arakawa, M., Ikeda, H., Wada, K., Mizuno, T., Hirose,
827 C., Hosoda, S., Mori, O., Shimada, T., Soldini, S., Tsukizaki, R., Yano, H., Ozaki, M.,
828 Takeuchi, H., Yamamoto, Y., Okada, T., Shimaki, Y., Shirai, K., Iijima, Y., Noda, H.,
829 Kikuchi, S., Yamaguchi, T., Ogawa, N., Ono, G., Mimasu, Y., Yoshikawa, K., Takahashi, T.,
830 Takei, Y., Fujii, A., Nakazawa, S., Terui, F., Tanaka, S., Yoshikawa, M., Saiki, T.,
831 Watanabe, S., Tsuda, Y., 2020. Sample collection from asteroid (162173) Ryugu by
832 Hayabusa 2: Implications for surface evolution. 2020. *Science*. 368, 654-659.
- 833 Nakamura, T., 2005. Post-hydration thermal metamorphism of carbonaceous chondrites. *Journal*
834 *of Mineralogical and Petrological Sciences*. 100, 260-272.
- 835 Newton, J., Bischoff, A., Arden, J.W., Franchi, I.A., Geiger, T., Greshake, A., Pillinger, C.T.,
836 1995. Acfer 094, a uniquely primitive carbonaceous chondrite from the Sahara. *Meteoritics*.
837 30, 47-56.
- 838 Nittler, L.R., Alexander, C. M. O'D., Foustoukos, D., Patzer, A., Verdier-Paoletti, M.J. 2020.
839 Asuka 12236, the most pristine cm chondrite to date (abstract). *Lunar and Planetary Science*.
840 51, 2276.

- 841 Noguchi, T., Yasutake, M., Tsuchiyama, A., Miyake, A., Kimura, M., Yamaguchi, A., Imae, N.,
842 Uesugi, K., Takeuchi, A. 2020. Matrix mineralogy of the least altered CM-related chondrite
843 Asuka 12169 (abstract). *Lunar and Planetary Science*. 51, 1666.
- 844 Quirico E, Raynal P-I, Bourot-Denise M., 2003. Metamorphic grade of organic matter in six
845 unequilibrated ordinary chondrites. *Meteoritics & Planetary Science*. 38, 795-881.
- 846 Quirico, E., Orthous-Daunay, F.-R., Beck, P., Bonal, L., Brunetto, R., Dartois, E., Pino, T.,
847 Montagnac, G., Rouzaud, J.-N., Engrand, C., Duprat, J., 2014. Origin of insoluble organic
848 matter in type 1 and 2 chondrites: New clues, new questions. *Geochimica et Cosmochimica*
849 *Acta*. 136, 80-99.
- 850 Rubin, A.E., 1998. Correlated petrologic and geochemical characteristics of CO₃ chondrites.
851 *Meteoritics & Planetary Science*. 33, 385-391.
- 852 Rubin, A.E., 2004. Aluminian low-Ca pyroxene in a Ca-Al-rich chondrule from the Semarkona
853 meteorite. *American Mineralogist*. 89, 867-872.
- 854 Rubin, A.E., 2015. An American on Paris: Extent of aqueous alteration of a CM chondrite and the
855 petrography of its refractory and amoeboid olivine inclusions. *Meteoritics & Planetary*
856 *Science*. 50, 1595-1612.
- 857 Rubin, A.E., Trigo-Rodríguez, J.M., Huber, H., Wasson, J.T., 2007. Progressive aqueous
858 alteration of CM carbonaceous chondrites. *Geochimica et Cosmochimica Acta*. 71,
859 2361-2382.
- 860 Russell, S.S., Huss, G.R., Fahey, A.J., Greenwood, R.C., Hutchison, R., Wasserburg, G.J., 1998.
861 An isotopic and petrologic study of calcium-aluminum-rich inclusions from CO₃ meteorites.
862 *Geochimica et Cosmochimica Acta*. 62, 689-714.

- 863 Schrader, D.L., Davidson, J., McCoy, T.J., 2016. Widespread evidence for high-temperature
864 formation of pentlandite in chondrites. *Geochimica et Cosmochimica Acta*. 189, 359-376.
- 865 Schrader, D.L., Davidson, J., 2017. CM and CO chondrites: A common parent body or asteroidal
866 neighbors? Insights from chondrule silicates. *Geochimica et Cosmochimica Acta*. 214,
867 157-171.
- 868 Scott, E.R.D., Krot, A.N., 2006. Thermal processing of silicate dust in the solar nebula: Clues from
869 primitive chondrite matrices. *Astrophysical Journal*. 623, 571-578.
- 870 Sears, D.W.G., Batchelor, J.D., Lu, J., Keck, B.D., 1991. Metamorphism of CO and CO-like
871 chondrites and comparisons with type 3 ordinary chondrites. *Proc. NIPR Symp. Antarct.*
872 *Meteorites*. 4, 319-343.
- 873 Singerling, S.A., Brearley, A.J., 2018. Primary iron sulfides in CM and CR carbonaceous
874 chondrites: Insights into nebular processes. *Meteoritics & Planetary Science*. 53, 2078-2106.
- 875 Starkey, N.A., Jackson, C.R.M., Greenwood, R.C., Parman, S., Franchi, I.A., Jackson, M., Fitton,
876 J.G., Stuart, F.M., Kurz, M., and Larsen, L.M., 2016. Triple oxygen isotopic composition of
877 the high $3\text{He}/4\text{He}$ mantle. *Geochimica et Cosmochimica Acta* 176, 227-238.
- 878 Stelzner, T., Heide, K., Bischoff, A., Weber, D., Scherer, P., Schultz, L., Happel, M., Schrön, W.,
879 Neupert, U., Michel, R., Clayton, R.N., Mayeda, T.K., Bonani, G., Haidas, I., Ivy-Ochs, S.,
880 Suter, M., 1999. An interdisciplinary study of weathering effects in ordinary chondrites from
881 the Acfer region, Algeria. *Meteoritics & Planetary Science*. 34, 787-794.
- 882 Tenner, T.J., Nakashima, D., Ushikubo, T., Tomioka, N., Kimura, M., Weisberg, M.K., Kita, N.T.,
883 2019. Extended chondrule formation intervals in distinct physicochemical environments:
884 Evidence from Al-Mg isotope systematics of CR chondrite chondrules with unaltered
885 plagioclase. *Geochimica et Cosmochimica Acta*. 260, 133-160.

- 886 Tsuchiyama, A., Noguchi, T., Yasutake, M., Miyake, A., Kimura, M., Yamaguchi, A., Imae, N.,
887 Uesugi, K., Takeuchi, A. 2020. Three-dimensional nano/microtexture of a least altered
888 CM-related chondrite Asuka 12169 (abstract). *Lunar and Planetary Science*. 51, 1801.
- 889 Van Schmus, W.R., Wood, J.A., 1967. A chemical-petrologic classification for the chondrite
890 meteorites. *Geochimica et Cosmochimica Acta*. 31, 747-765.
- 891 Wasson, J.T., Rubin, A.E., 2010. Matrix and whole-rock fractionations in the Acfer 094 type 3.0
892 ungrouped carbonaceous chondrite. *Meteoritics & Planetary Science*. 45, 73-90.
- 893 Weisberg, M.K., McCoy, T.J., Krot, A.N., 2006. Systematics and evaluation of meteorite
894 classification. in: Lauretta, D.S., McSween, H.Y., Jr. (Eds.), *Meteorites and the Early Solar*
895 *System II*. The University of Arizona Press, Tucson, pp. 19-52.
- 896 Wolf, D., Palme, H., 2001. The solar system abundances of phosphorus and titanium and the
897 nebular volatility of phosphorus. *Meteoritics & Planetary Science*. 36, 559-571.
- 898 Yamaguchi, A., Barrat, J.-A., Ito, M., Bohn, M., 2011. Post-impact magmatism on Vesta:
899 Evidence from the petrology and thermal history of diogenites. *Journal of Geophysical*
900 *Research*. 116, E08009, 15 PP., 2011, <https://doi:10.1029/2010JE003753>.
- 901 Yamaguchi, A., Kimura, M., Pittarello, L., Imae, N., Debaille, V., Philippe, C., Kojima, H. 2016.
902 *Meteorite Newsletter*. 25.
- 903 Zolensky, M., Barrett, R., Browning, L., 1993. Mineralogy and composition of matrix and
904 chondrule rims in carbonaceous chondrites. *Geochimica et Cosmochimica Acta*. 57,
905 3123-3148.
- 906 Zolensky, M.E., Weisberg, M.K., Buchanan, P.C., Mittlefehldt, D.W., 1996. Mineralogy of
907 carbonaceous chondrite clast in HED achondrites and the Moon. *Meteoritics & Planetary*
908 *Science*. 31, 518-537.

909

910

Journal Pre-proof

911 **Figure captions**

912 Fig. 1. Backscattered electron (BSE) images of a) A 12085, 41-1 (width of sample 12.8 mm),
913 showing chondrules among matrix), b) A 12169, 31-1 (6.7 mm), containing fusion crusts in
914 both sides of the section (gray areas), and c) combined elemental (Mg-Ca-Al) map of A
915 12169 showing CAIs, and d) BSE image of A 12236, 51-1 (12.6 mm).

916 Fig. 2. BSE images of constituent components. a) A melilite (Mel) -rich CAI with spinel (Sp) and
917 high-Ca pyroxene (Hpx) in A 12169. The width is 210 μm . b) An AOA, consisting of
918 forsteritic olivine (Ol) with interstitial anorthite and high-Ca pyroxene (An+Hpx) and
919 kamacite (Kam) in A 12236. The width is 280 μm . c) A Type I chondrule in A 12169,
920 mainly consisting of phenocrysts of olivine and low-Ca pyroxene (Lpx), among feldspathic
921 mesostasis (light gray). The width is 0.76 mm. d) A Type I chondrule in A 12169
922 consisting of olivine, low- and high-Ca pyroxene, and glassy mesostasis (Gla). The width
923 is 240 μm . e) A type II chondrule in A 12085, consisting of ferroan olivine with abundant
924 relict forsteritic olivine (dark), surrounded by fine-grained rim. The width is 0.65 mm. f) A
925 peripheral part of type I chondrule in A 12085. Mesostasis is replaced by phyllosilicate
926 (Phy). The width is 170 μm . g) Homogeneous kamacite spherules in a type I chondrule of
927 A 12236. The width is 210 μm . h) A matrix area of A 12169, consisting of very
928 fine-grained silicate phases with abundant sulfide of submicron in size (bright). The width
929 is 20 μm . i) A sulfide grain in A 12169, consisting of pyrrhotite (Po) with small amounts of
930 pentlandite (Pn). The width is 190 μm . j) A type I chondrule and matrix area of A 12085,
931 including fine-grained aggregates of Fe-sulfide with silicate phases (Sul+Sil). The width is
932 210 μm .

- 933 Fig. 3. Olivine compositions. a) Fe vs. Mn plot of olivine from the Asuka chondrites, in
 934 comparison with that of Murchison (CM2.5). b) Mean Cr_2O_3 vs. $\sigma\text{-Cr}_2\text{O}_3$ plot in ferroan
 935 olivine for Asuka chondrites. The diagram and CO trend are after Grossman and Brearley
 936 (2005) and Schrader and Davidson (2017). A dotted circle shows the area of CO3.0 and
 937 CM chondrites.
- 938 Fig. 4. The mesostasis composition on (Si+Al)-Mg-Fe diagram (atomic ratio) for the Asuka
 939 chondrites and other CM and CO chondrites.
- 940 Fig. 5. Ni vs. Co (wt.%) plot of Fe-Ni metal grains in the Asuka chondrites. The dotted line shows
 941 the CI chondritic Co/Ni ratio after Anders and Grevesse (1989).
- 942 Fig. 6. Matrix compositions of the Asuka chondrites in atomic (Si+Al)-Mg-Fe plot, compared with
 943 other CMs, COs, and Acfer 094 (this work; Metzler et al., 1992; Zolensky et al., 1993;
 944 Marrocchi et al., 2014; Wasson and Rubin, 2010).
- 945 Fig. 7. a) X-ray diffraction of 2 theta, 0-30° for the Asuka chondrites, in comparison with A 12248
 946 (CM2.0). b) Diffraction of 2 theta, 29-33.5°. c) Diffraction of 2 theta, 42.8-45.2°.
 947 Ant=antigolite, Cro=cronstedtite, Cen=clinoenstatite, Fa=fayalitic olivine, Kam=kamacite,
 948 Oen=orthoenstatite, Tae=taenite, Toc=tochilinite, and Tr=troilite.
- 949 Fig. 8. Spectral parameters of Raman bands of carbonaceous matter from the matrix of the Asuka
 950 chondrites and Murchison. Dotted areas summarize data from the other chondrites. CRs,
 951 COs, CVs, and UOCs are after Komatsu et al. (2018). CMs-B is after Buseman et al.
 952 (2007), and CRs&CMs-Q is after Quirico et al. (2014).
- 953 Fig. 9. a) Al/Mn versus (Zn/Mn)x100 atomic ratios of the Asuka chondrites. Dotted areas for
 954 chondrites are after Krot et al. (2014). b) The CI-normalized bulk composition of A 12236
 955 (CM2.9), compared with those of Paris (CM2.7), Murchison (CM2.5), Nogoya (CM2.2),

956 NWA 11024 (dehydrated CM), and CM-mean. The data of Paris and Nogoya are after
957 Hewins et al. (2014), Murchison after Wolf and Palme (2001) and Hewins et al. (2014),
958 NWA 11024 after Ebert et al. (2019), and CM-mean after Lodders and Fegley (1998). In
959 NWA 11024, the data of Sr, Ba, and U, are not plotted because of terrestrial weathering
960 effect (Stelzner et al., 1999). The condensation temperatures for elements are after Lodders
961 and Fegley (1998).

962 Fig. 10. Oxygen three isotope diagram showing the relationship between the Asuka CMs,
963 anomalous C2 chondrites, “normal” CM2 chondrites and CO3 chondrites. The regression
964 line shown was calculated using only the analyses of anomalous C2 samples. TFL =
965 Terrestrial Fractionation Line. CCAM = Carbonaceous Chondrite Anhydrous Mineral line
966 (Clayton and Mayeda, 1999). Data sources – “normal” CM2s: Clayton and Mayeda, 1999);
967 Haack et al., 2012; Hewins et al., 2014, CO3 chondrite falls: Alexander et al. (2018);
968 Anomalous C2 chondrites Clayton and Mayeda, 1999; with the exception of: EET 85311
969 “OU” and EET 85311 “AK” (Lee et al., 2016); LEW 85311 “Lee” (Lee et al., 2019); NWA
970 5958 (Jacquet et al., 2016).

971

Table 1. Modal abundance (vol. %) of components in A 12085, A 12169, and A 12236, compared with other CMs.

Sample	Subtype	Chondrule	Refractory inclusion	Matrix	Metal	Sulfide	References
A 12085	2.8	36.0	4.2	57.7	1.2	0.9	<i>This work</i>
A 12169	3.0	38.6	4.3	53.4	2.3	1.4	<i>This work</i>
A 12236	2.9	28.9	3.8	64.8	1.5	1.1	<i>This work</i>
Paris	2.7	<45	<1	55	1.2	0.7	<i>Hewins et al. (2014); Rubin (2015)</i>
EET 96029	2.7	17	1.8	78	0.3	1.2	<i>Lee et al. (2016)</i>
NWA 11024	"3.0"	32	1.2	64	2.4	0.5	<i>Ebert et al. (2019)</i>
CM		20	5	70	0.1		<i>Weisberg et al. (2016)</i>

Table 2. Characteristic features of chondrules in A 12085, A 12169, and A 12236, compared with other CMs.

Sample	Average diameter (mm)	Porphyritic chondrules (%)	Type I chondrule ¹⁾ (%)	Alteration (%) ²⁾			References
				completely	partially	unaltered	
A 12085	0.31	97.5	90.3	22	56	22	<i>This work</i>
A 12169	0.26	95.2	92.2	0	36	64	<i>This work</i>
A 12236	0.29	97.9	91.8	2	50	48	<i>This work</i>
Paris	0.25						<i>Hewins et al. (2014); Rubin (2015)</i>
EET 96029	0.4						<i>Lee et al. (2016)</i>
NWA 11024	0.15-0.3						<i>Ebert et al. (2019)</i>
CM	0.3	95	90-90				<i>Weisberg et al. (2006); Jones (2012)</i>

¹⁾ Percentage of Type I
in all chondrules.

²⁾ See alteration degree in the text.

Table 3. Representative compositions of silicate and oxide phases and the average matrix composition.

Phase	Sample	Occurrence	Type	SiO ₂	TiO ₂	Al ₂ O ₃	Cr ₂ O ₃	V ₂ O ₃	FeO	NiO	MnO	MgO	CaO	ZnO	Na ₂ O	K ₂ O	P ₂ O ₅	SO ₃	Total	Wo	En	Fs	An	Ab	Or
Feldspar	A 12169	Chondrule	I	46.44	b.d.	33.53	b.d.	b.d.	0.30	b.d.	0.10	0.77	19.61	b.d.	0.05	b.d.	b.d.	b.d.	100.81				99.4	0.4	0.2
Feldspar	A 12236	Chondrule	II	64.02	0.05	23.08	b.d.	b.d.	1.02	b.d.	b.d.	0.13	4.45	b.d.	8.66	0.30	b.d.	b.d.	101.71				21.7	76.6	1.7
Feldspar	A 12236	AOA		42.94	0.17	36.14	b.d.	b.d.	0.37	b.d.	b.d.	0.72	20.18	b.d.	b.d.	b.d.	b.d.	b.d.	100.51				99.8	0.2	0.0
Glass	A 12169	Chondrule	I	51.60	0.06	24.40	0.24	b.d.	1.25	b.d.	b.d.	8.42	13.75	b.d.	1.55	0.10	b.d.	b.d.	101.36				82.5	16.9	0.7
Melilite	A 12085	CAI		22.38	0.15	35.55	b.d.	b.d.	0.11	b.d.	b.d.	0.54	40.91	b.d.	b.d.	b.d.	b.d.	b.d.	99.63						
Olivine	A 12085	Chondrule	I	42.51	0.09	0.16	0.18	b.d.	0.11	b.d.	b.d.	56.78	0.42	b.d.	b.d.	b.d.	b.d.	b.d.	100.24						
Olivine	A 12085	Chondrule	II	37.05	b.d.	b.d.	0.30	b.d.	31.90	b.d.	0.26	30.85	0.32	b.d.	b.d.	b.d.	b.d.	b.d.	100.67						
Olivine	A 12085	AOA		42.87	0.09	b.d.	0.29	b.d.	0.26	b.d.	0.36	56.48	0.05	b.d.	b.d.	b.d.	b.d.	b.d.	100.40						
Phyllosilicate	A 12085	Chondrule	I	39.55	0.05	1.92	0.35	b.d.	20.92	0.26	0.65	14.85	1.60	b.d.	0.34	0.18	b.d.	1.07	81.72						
Phyllosilicate	A 12236	Chondrule	I	31.15	b.d.	12.68	b.d.	b.d.	31.88	b.d.	0.14	8.36	0.16	b.d.	0.29	0.27	0.17	0.36	85.45						
Merrillite	A 12085	Chondrule	II	0.62	0.08	0.47	b.d.	b.d.	2.21	b.d.	0.10	2.97	45.05	b.d.	2.67	b.d.	44.32	0.46	98.94						
High-Ca pyroxene	A 12085	Chondrule	I	52.45	0.51	4.28	1.01	b.d.	2.22	b.d.	0.36	25.01	13.02	b.d.	b.d.	b.d.	b.d.	b.d.	98.85	26.3	70.2	3.5			
High-Ca pyroxene	A 12236	Chondrule	II	51.03	0.16	0.62	1.03	b.d.	17.14	b.d.	0.36	11.01	16.89	b.d.	0.43	b.d.	b.d.	b.d.	98.66	37.1	33.6	29.4			
Kushiroite	A 12169	CAI		31.30	0.13	37.95	b.d.	b.d.	2.30	b.d.	b.d.	3.34	26.32	b.d.	b.d.	b.d.	b.d.	b.d.	101.33						
Low-Ca pyroxene	A 12169	Chondrule	I	58.80	0.28	0.99	0.40	b.d.	0.52	b.d.	0.08	37.53	0.54	b.d.	b.d.	b.d.	b.d.	b.d.	99.13	1.0	98.2	0.8			
Low-Ca pyroxene	A 12169	Chondrule	II	49.92	b.d.	0.13	0.43	b.d.	34.78	b.d.	0.28	12.48	0.40	b.d.	b.d.	b.d.	b.d.	b.d.	98.41	0.9	38.7	60.5			
Chromite	A 12085	Chondrule	II	0.25	0.96	9.24	54.56	0.64	26.96	b.d.	0.38	6.38	0.02	0.11	b.d.	b.d.	b.d.	b.d.	99.49						
Spinel	A 12169	AOA		b.d.	0.19	72.13	b.d.	0.18	0.25	b.d.	b.d.	27.54	0.20	b.d.	b.d.	b.d.	b.d.	b.d.	100.50						
Matrix	A 12085	Matrix		29.04	0.06	2.65	0.37	b.d.	28.46	1.80	0.23	15.90	0.68	b.d.	0.23	0.11	0.12	11.44	91.10						
Matrix	A 12169	Matrix		31.29	0.07	2.60	0.38	b.d.	29.63	1.74	0.24	17.48	0.81	b.d.	0.49	0.15	0.22	10.71	95.80						
Matrix	A 12236	Matrix		29.35	0.07	2.57	0.35	b.d.	30.03	1.76	0.24	15.43	0.59	b.d.	0.21	0.12	0.19	9.06	89.97						

b.d.: below detection limits (3 sigma), 0.03 for SiO₂, Al₂O₃, MgO, CaO, and SO₃, 0.04 for TiO₂, V₂O₃, Na₂O, K₂O, and P₂O₅, 0.08 for NiO and MnO, and 0.10 for Cr₂O₃ and ZnO.

* Matrix data was averaged composition.

Table 4. Representative compositions of opaque minerals.

Phase	Sample	Occurrence	Si	P	S	Cr	Fe	Co	Ni	Cu	Total
Kamacite	A 12085	Isolated	b.d.	0.18	b.d.	b.d.	93.25	0.29	5.42	0.07	99.21
Kamacite	A 12085	Chondrule	0.58	0.39	b.d.	0.99	92.81	0.28	4.88	b.d.	99.92
Kamacite	A 12236	Chondrule	b.d.	0.33	b.d.	0.33	92.33	0.33	5.50	0.08	98.89
Kamacite	A 12236	Chondrule	b.d.	0.35	b.d.	0.20	93.31	0.33	5.60	0.00	99.79
Ni-rich metal	A 12085	Chondrule	b.d.	b.d.	b.d.	b.d.	67.26	2.14	29.83	b.d.	99.23
Ni-rich metal	A 12169	Isolated	b.d.	b.d.	b.d.	b.d.	55.76	2.02	40.27	0.06	98.11
Ni-rich metal	A 12236	Isolated	b.d.	b.d.	b.d.	0.06	66.09	2.11	30.86	b.d.	99.12
Pentlandite	A 12169	Isolated	b.d.	b.d.	32.77	b.d.	34.41	0.93	30.62	0.20	98.93
Pentlandite	A 12236	Chondrule	b.d.	b.d.	32.73	b.d.	38.63	0.89	25.78	0.07	98.10
Pyrrhotite	A 12169	Isolated	b.d.	b.d.	36.87	b.d.	60.53	0.14	0.68	b.d.	98.21
Pyrrhotite	A 12236	Isolated	b.d.	b.d.	36.95	b.d.	58.76	0.33	2.28	b.d.	98.32
Troilite	A 12169	Isolated	b.d.	b.d.	35.69	b.d.	61.68	0.07	0.40	b.d.	97.84
Troilite	A 12236	Isolated	b.d.	b.d.	36.32	b.d.	62.10	0.08	0.24	b.d.	98.74

b.d.: below detection limits (3 sigma), 0.03 for Si and P, and 0.05 for S, Co, Ni, Cr, Fe, and Cu.

Table 5. Major and trace element abundances for A 12236.

ICP-AES			ICP-MS			ICP-MS		
TiO ₂	wt%	0.11	Li	μg/g	1.72	La	μg/g	0.325
Al ₂ O ₃	wt%	2.17	Be	μg/g	0.0286	Ce	μg/g	0.830
FeO	wt%	30.25	CaO	wt%	1.75	Pr	μg/g	0.126
MnO	wt%	0.23	P ₂ O ₅	wt%	0.24	Nd	μg/g	0.636
MgO	wt%	19.95	K	μg/g	383	Sm	μg/g	0.208
CaO	wt%	1.77	Sc	μg/g	8.88	Eu	μg/g	0.0785
Na ₂ O	wt%	0.37	TiO ₂	wt%	0.0987	Gd	μg/g	0.286
K ₂ O	wt%	0.04	V	μg/g	66.78	Tb	μg/g	0.0537
P ₂ O ₅	wt%	0.23	Mn	μg/g	1597	Dy	μg/g	0.364
Ni	wt%	1.36	Co	μg/g	558	Ho	μg/g	0.0809
Cr	μg/g	3177	Cu	μg/g	111	Er	μg/g	0.238
			Zn	μg/g	162	Tm	μg/g	0.0358
			Ga	μg/g	7.46	Yb	μg/g	0.227
			Rb	μg/g	1.90	Lu	μg/g	0.0352
			Sr	μg/g	9.89	Hf	μg/g	0.153
			Y	μg/g	2.27	Ta	μg/g	0.0187
			Zr	μg/g	5.15	W	μg/g	0.14
			Nb	μg/g	0.381	Pb	μg/g	1.26
			Cs	μg/g	0.103	Th	μg/g	0.0398
			Ba	μg/g	3.22	U	μg/g	0.00957

Table 6. Petrologic subtypes of CM chondrites, modified after Rubin (2015).

Petrologic subtype	3.0	2.9	2.8	2.7	2.6	2.5	2.4	2.3	2.2	2.1	2.0
Chondrule mesostases	Primary meso Rare Phyllo	Primary meso □ Phyllo	Phyllo>Primary meso	Phyllosilicate	Phyllosilicate	Phyllosilicate	Phyllosilicate	Phyllosilicate	Phyllosilicate	Phyllosilicate	Phyllosilicate
Matrix phyllosilicates	Rare or no	Rare	Minor	Abundant	Abundant	Abundant	Abundant	Abundant	Abundant	Abundant	Abundant
Matrix composition: MgO/"feo"	>0.5	>0.5	>0.5	0.35-0.43	0.35-0.43	0.35-0.43	0.35-0.43	0.50-0.70	0.50-0.70	0.50-0.70	0.50-0.70
Matrix composition: S/SiO ₂	>0.1	>0.1	>0.1	0.10-0.18	0.10-0.18	0.10-0.16	0.10-0.16	0.07-0.08	0.07-0.08	0.05-0.07	0.05-0.07
Metallic Fe-Ni (vol%)	>2	1-2	1-2	1-2	~1	0.03-0.30	0.03-0.30	0.03-0.30	0.03-0.30	≤0.02	≤0.02
Phenocrysts in chondrules	Unaltered	Unaltered	Unaltered	Unaltered	Unaltered	Unaltered	Unaltered	2-15% altered	15-85% altered	85-99% altered	Completely altered
Large TCI clumps (vol%)	No TCI	No TCI	Minor	5-20	15-40	15-40	15-40	15-40	15-40	2-5	2-5
TCI composition: "FeO"/SiO ₂				4.0-7.0	2.0-3.3	2.0-3.3	1.5-2.0	1.5-2.0	1.0-1.7	1.0-1.7	1.0-1.7
TCI composition: S/SiO ₂				0.40-0.60	0.18-0.35	0.18-0.35	0.14-0.20	0.14-0.20	0.05-0.09	0.05-0.09	0.05-0.09
Sulfide	Tro > po + pn	Tro > po + pn	Tro > po + pn	po + pn	Mainly Po + pn	Mainly Po + pn	po + pn + int	po + pn + int	Mainly pn + int	Mainly pn + int	Mainly pn + int
Carbonate	No or rare carbonate	No or rare carbonate	Minor	Ca carbonate	Ca carbonate	Ca carbonate	Ca carbonate	Ca carbonate	Ca carbonate	Ca carbonate + complex carbonate	Ca carbonate + complex carbonate

Primary meso: primary feldspar and glass, tro: troilite, po: pyrrhotite, pn: pentlandite, int: sulfide grains with "intermediate" Ni/(Fe + Ni) ratios
Subtypes 2.7-2.0 are after Rubin (2015).

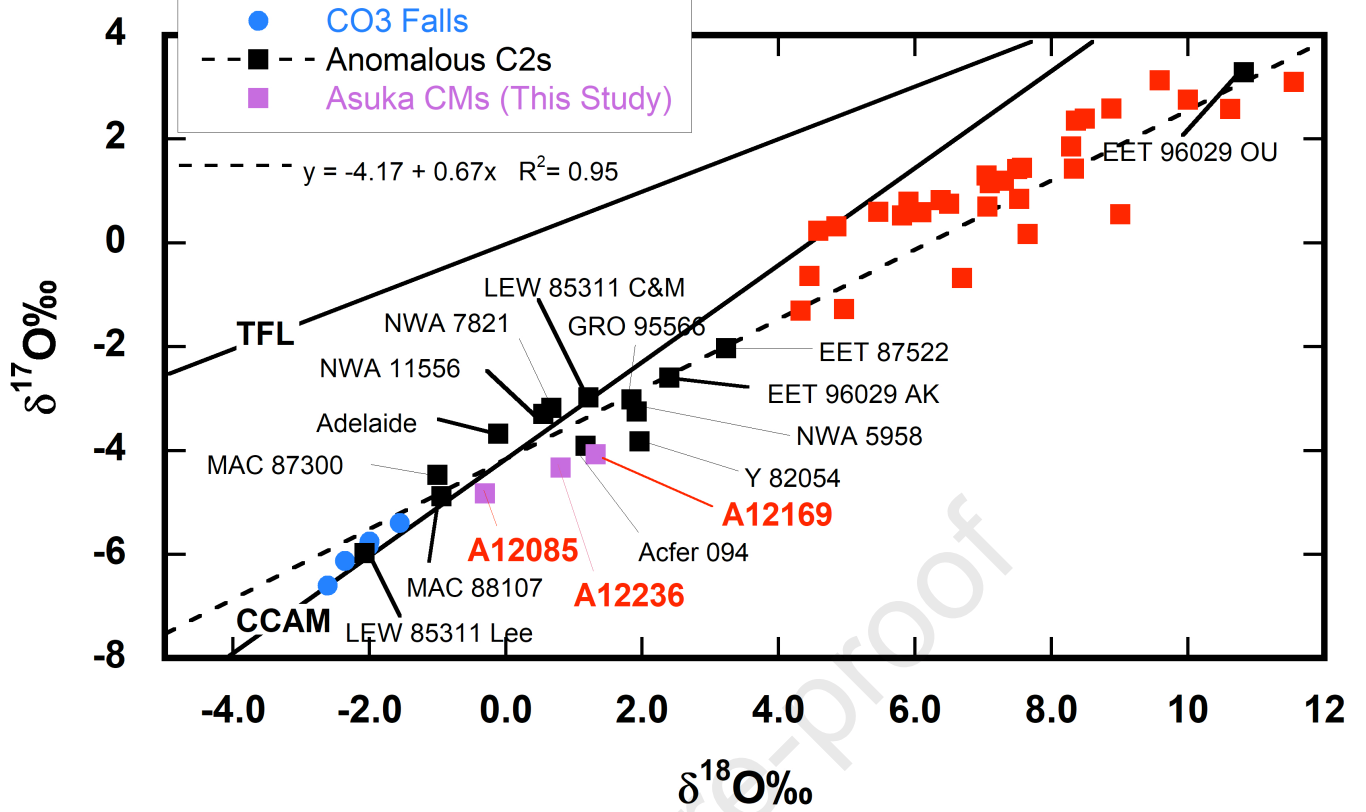


Fig. 10

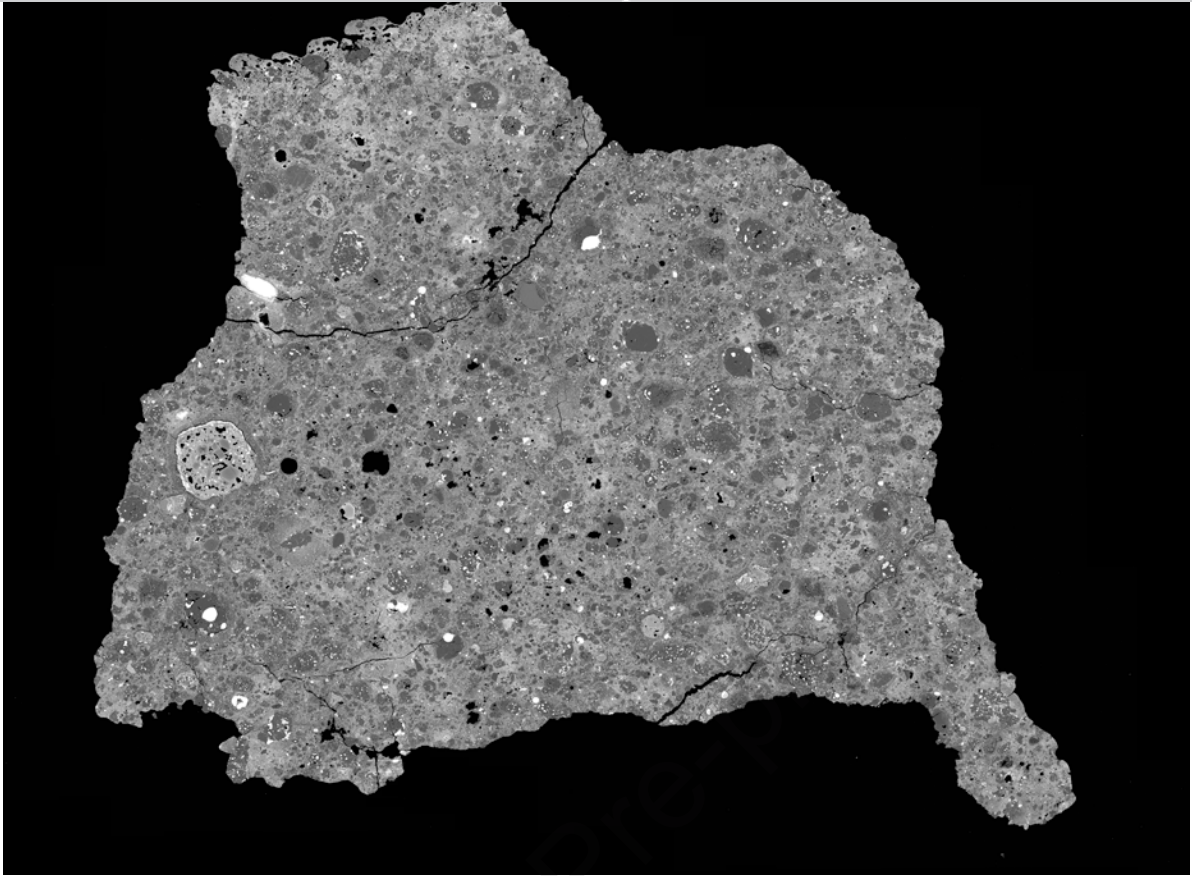


Fig. 1a

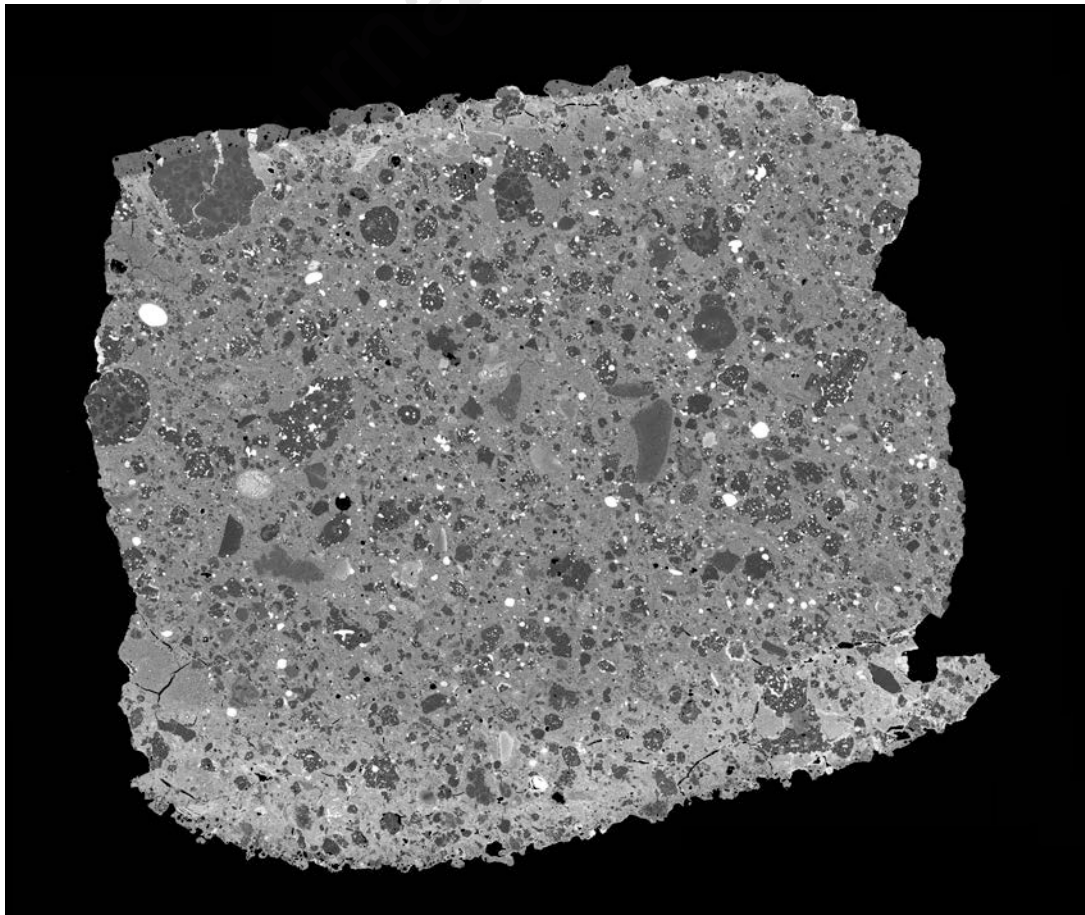


Fig. 1b

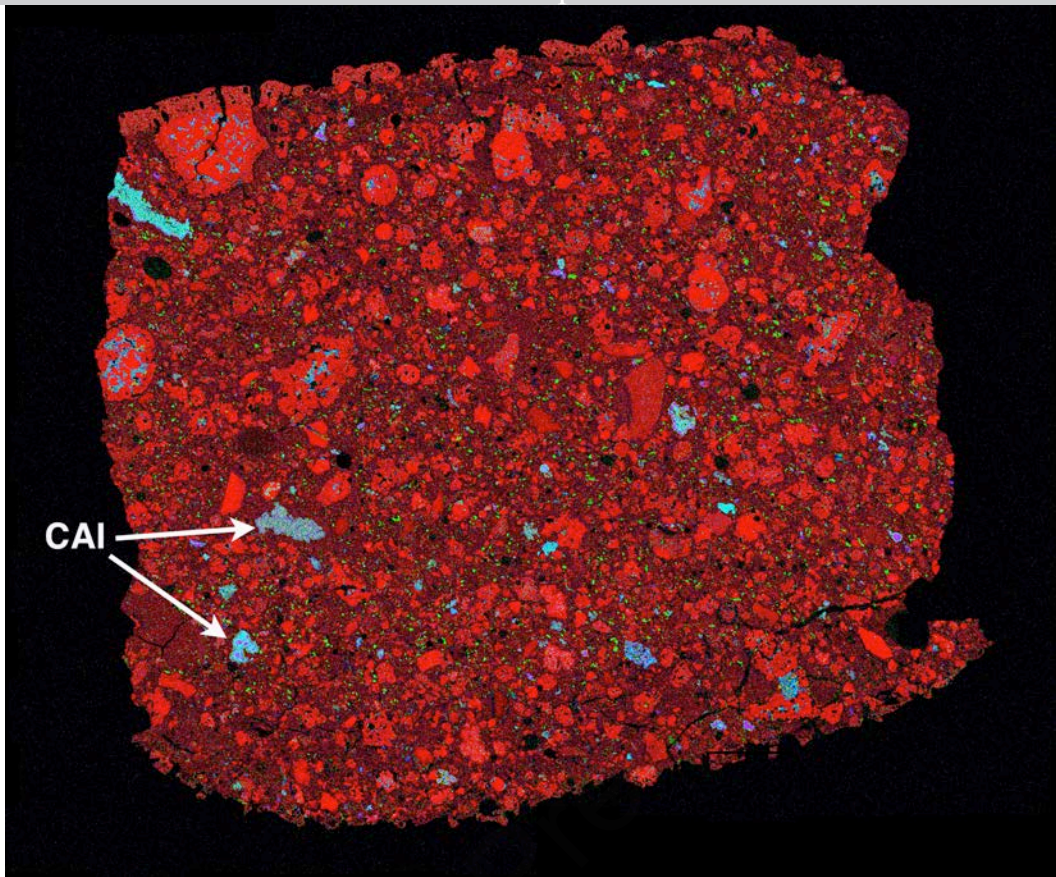


Fig. 1c

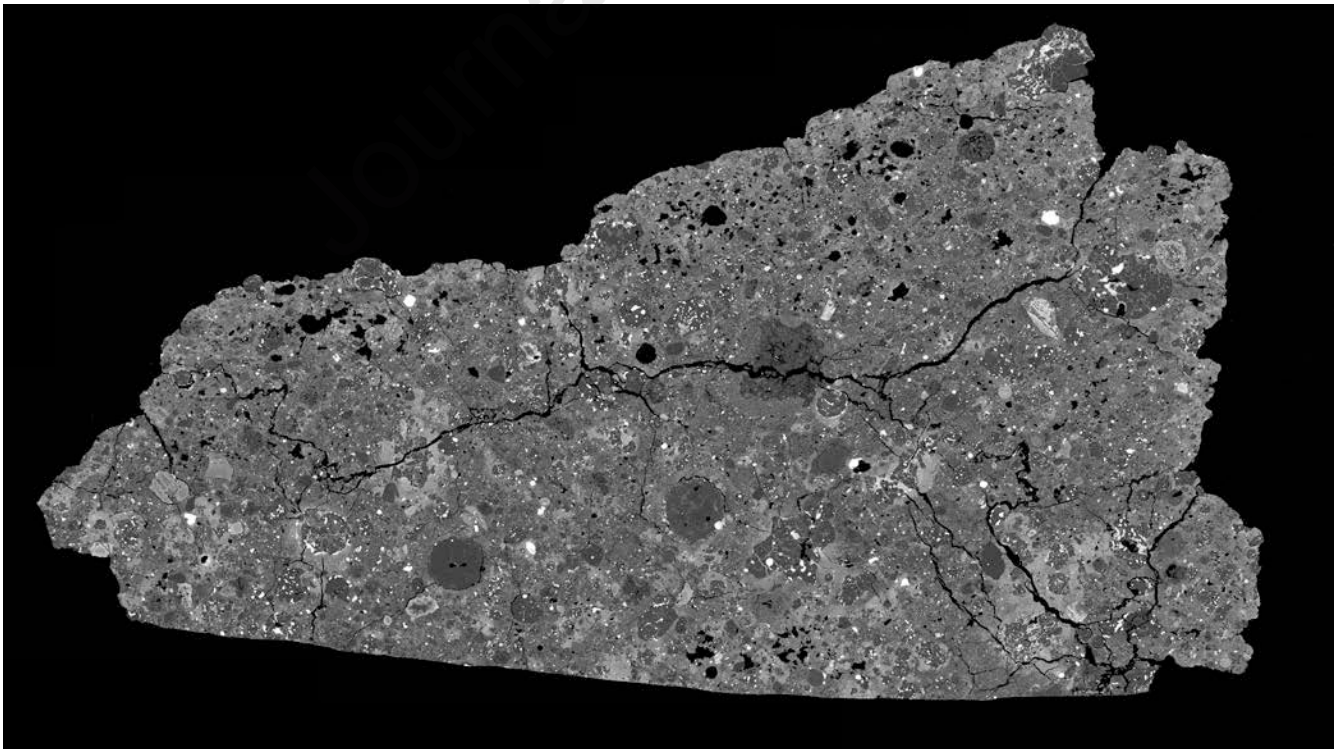


Fig. 1d

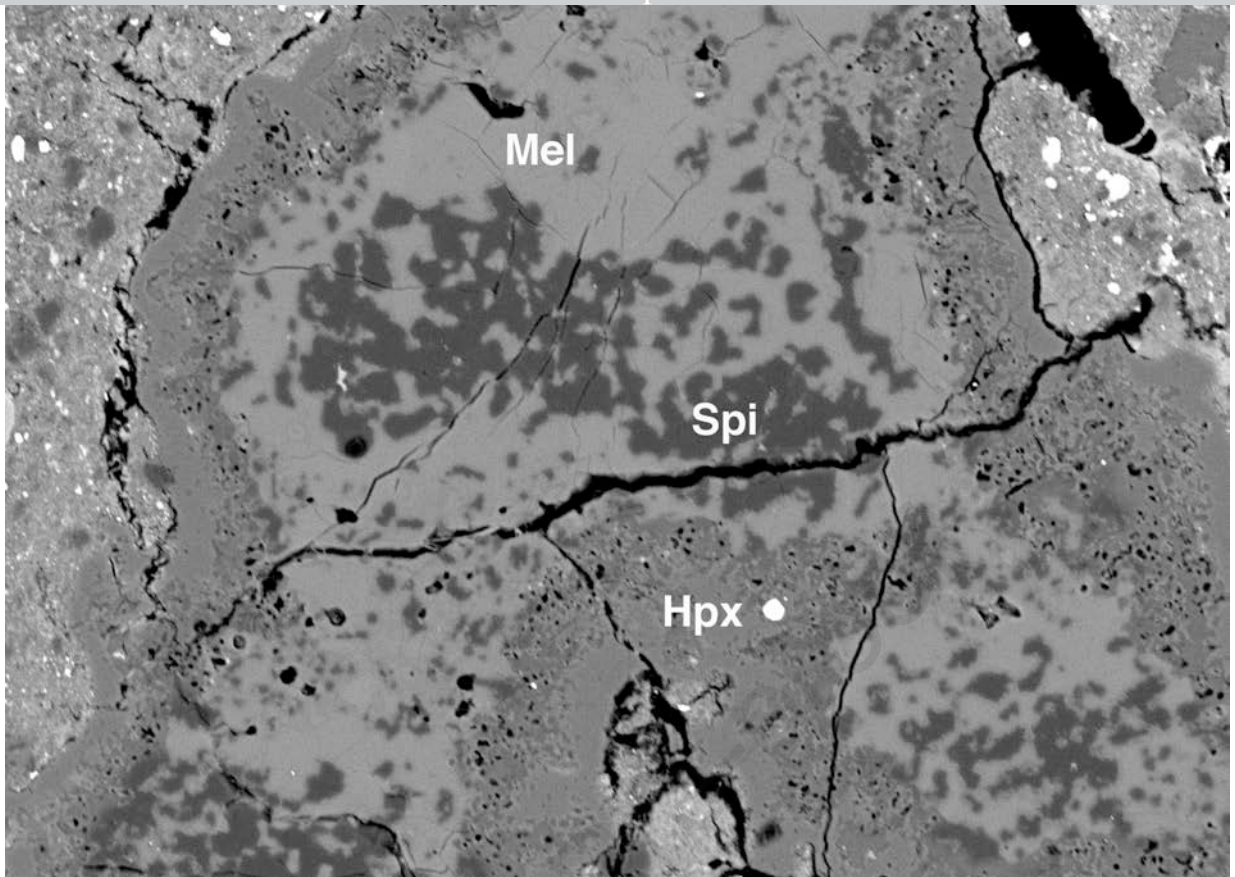


Fig. 2a

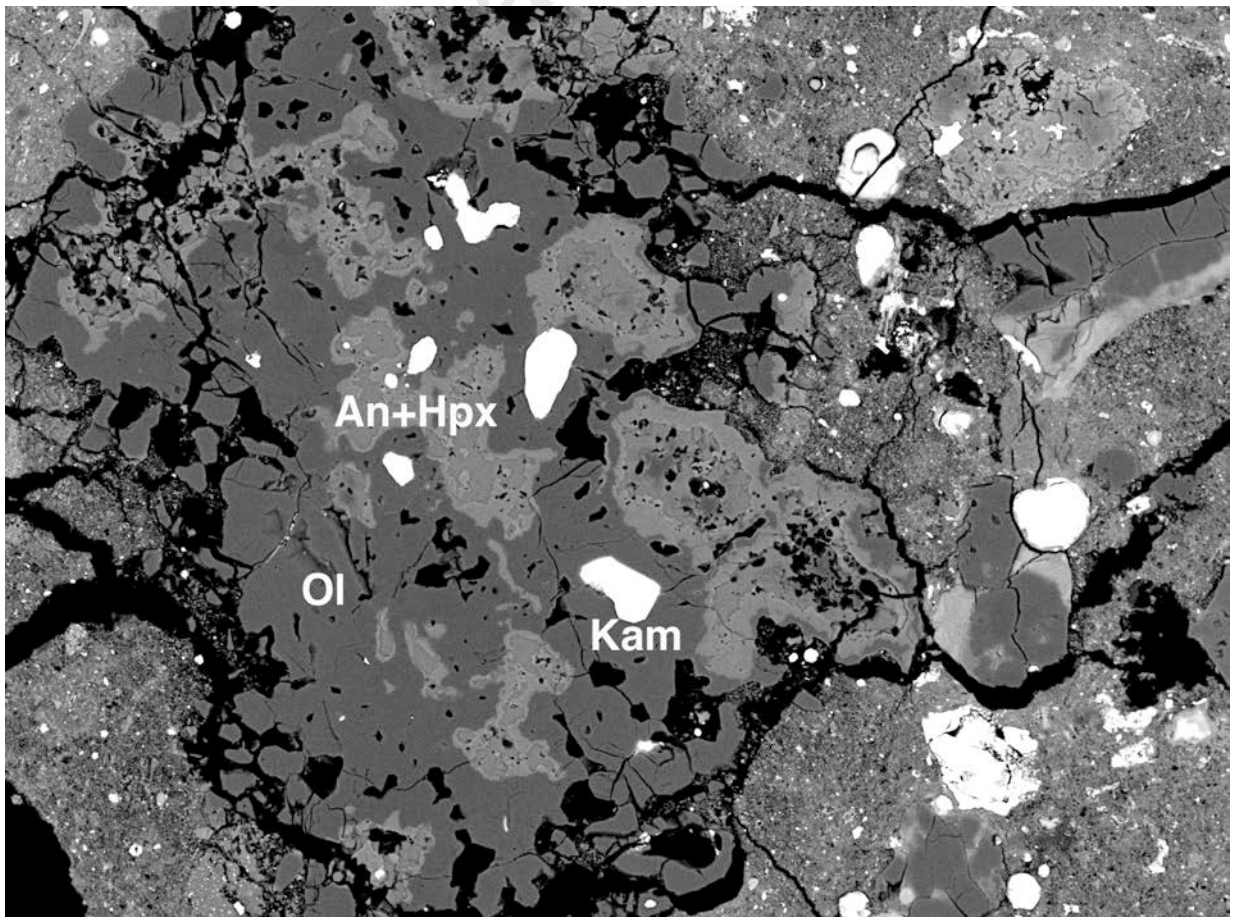


Fig. 2b

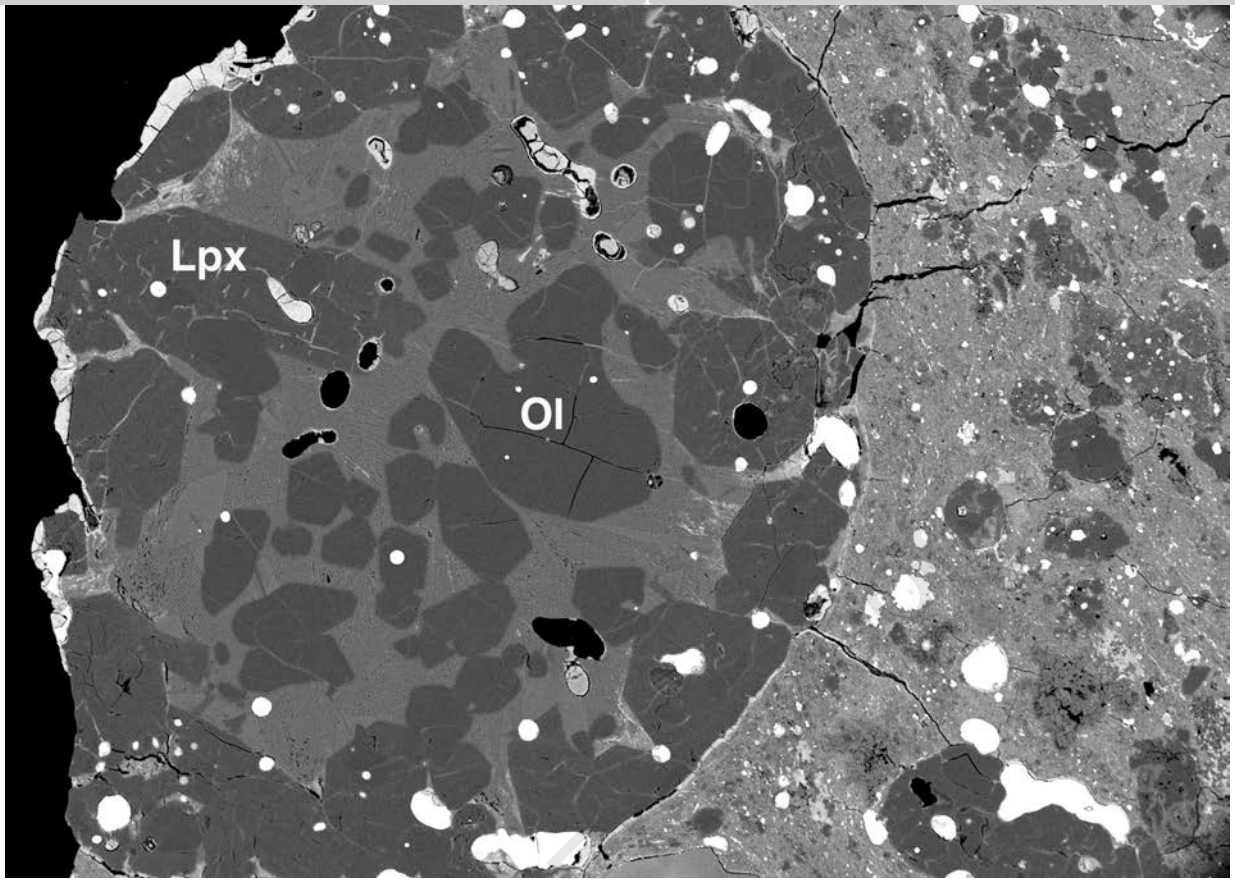


Fig. 2c

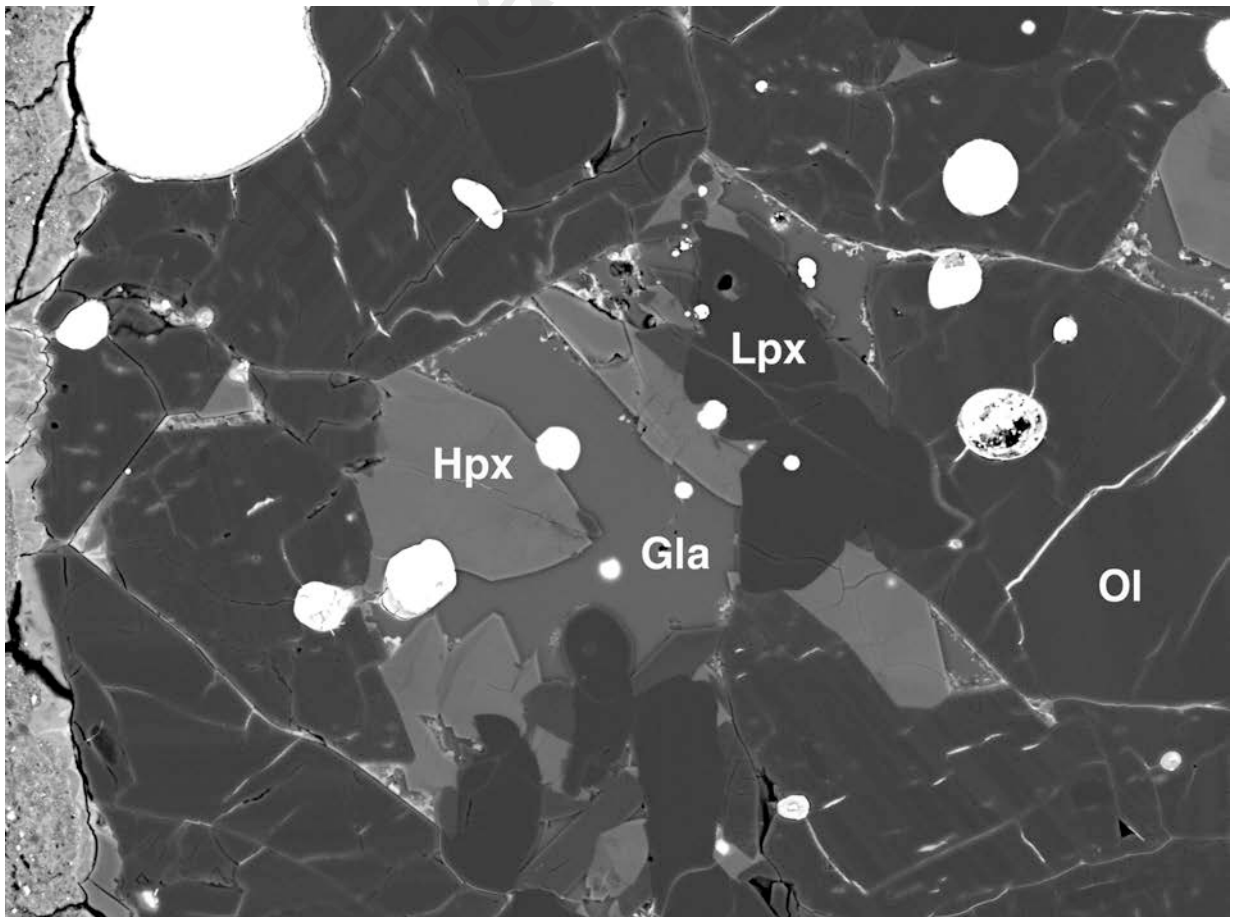


Fig. 2d

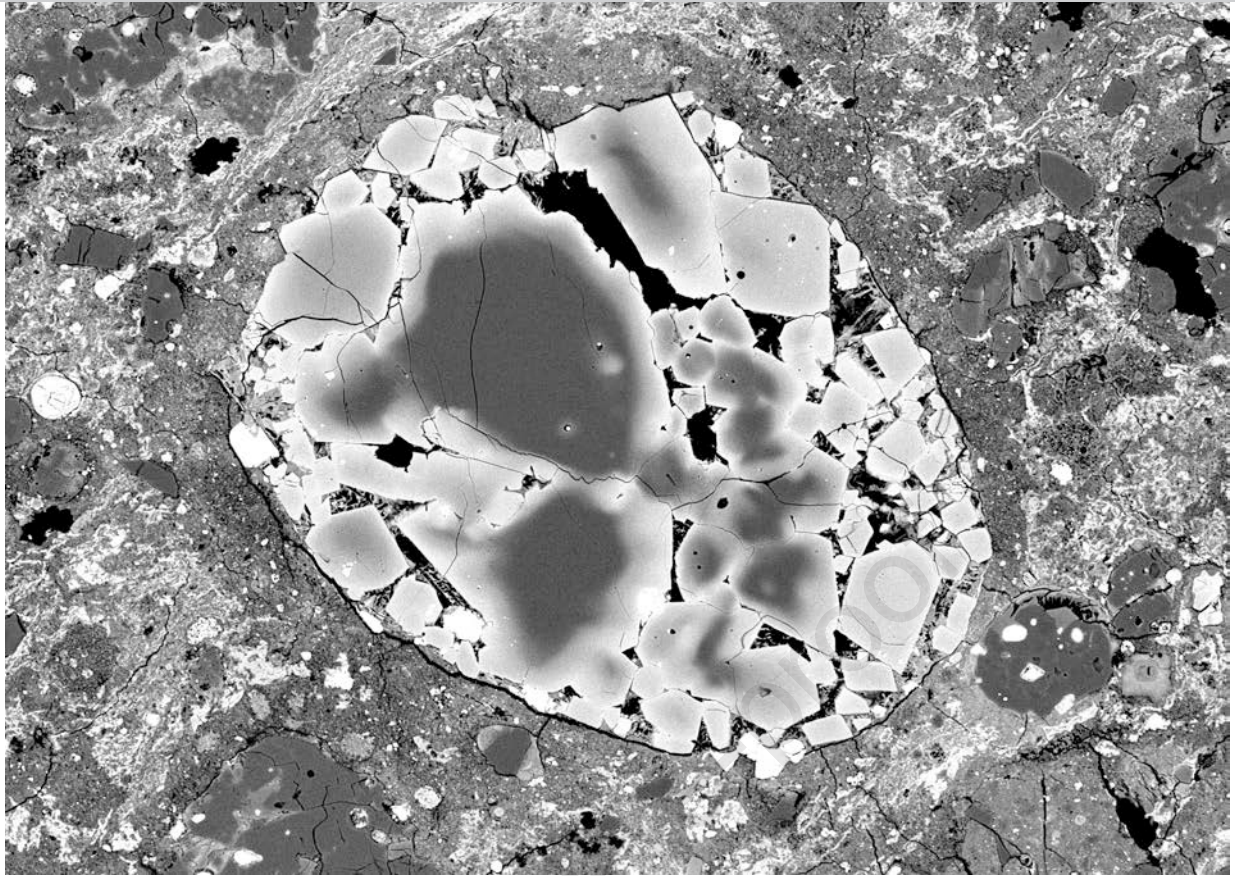


Fig. 2e

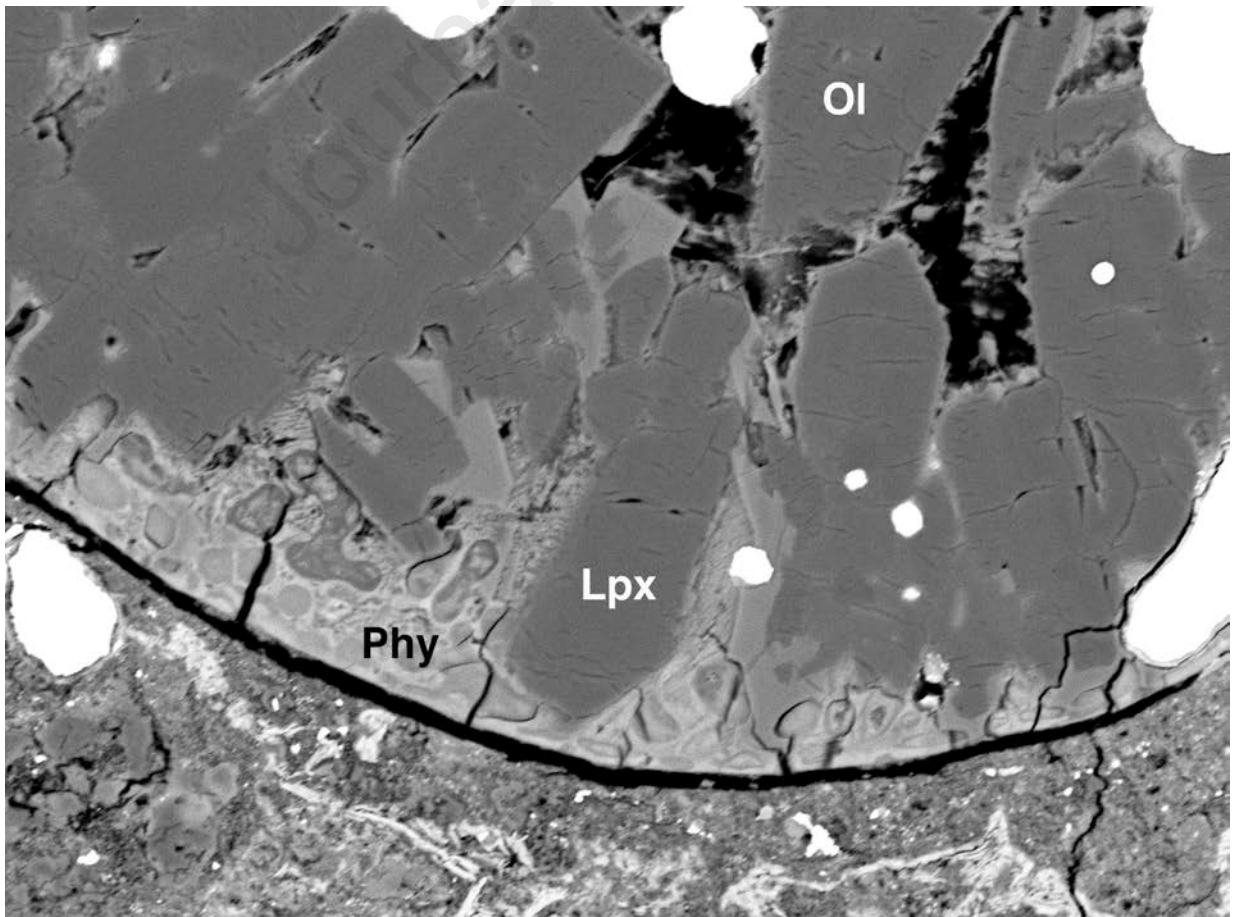


Fig. 2f

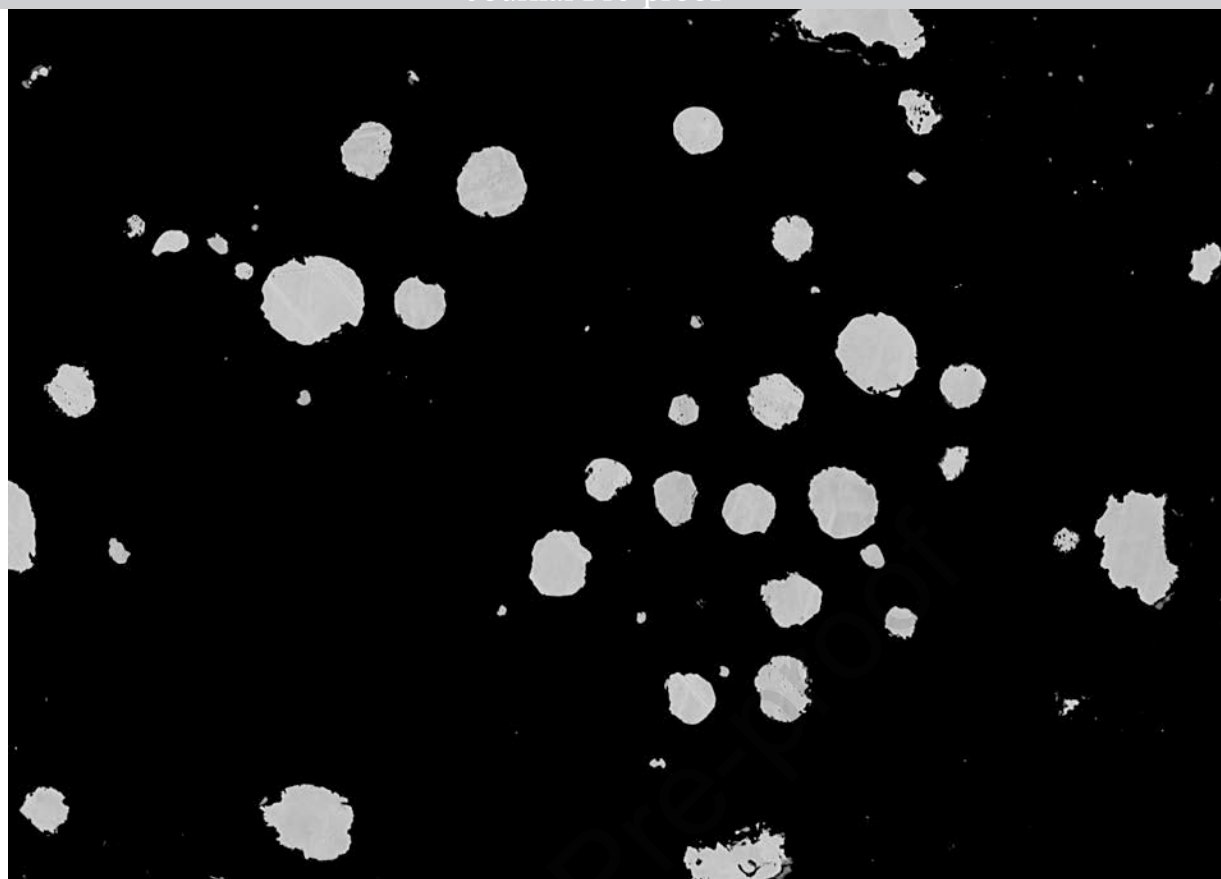


Fig. 2g

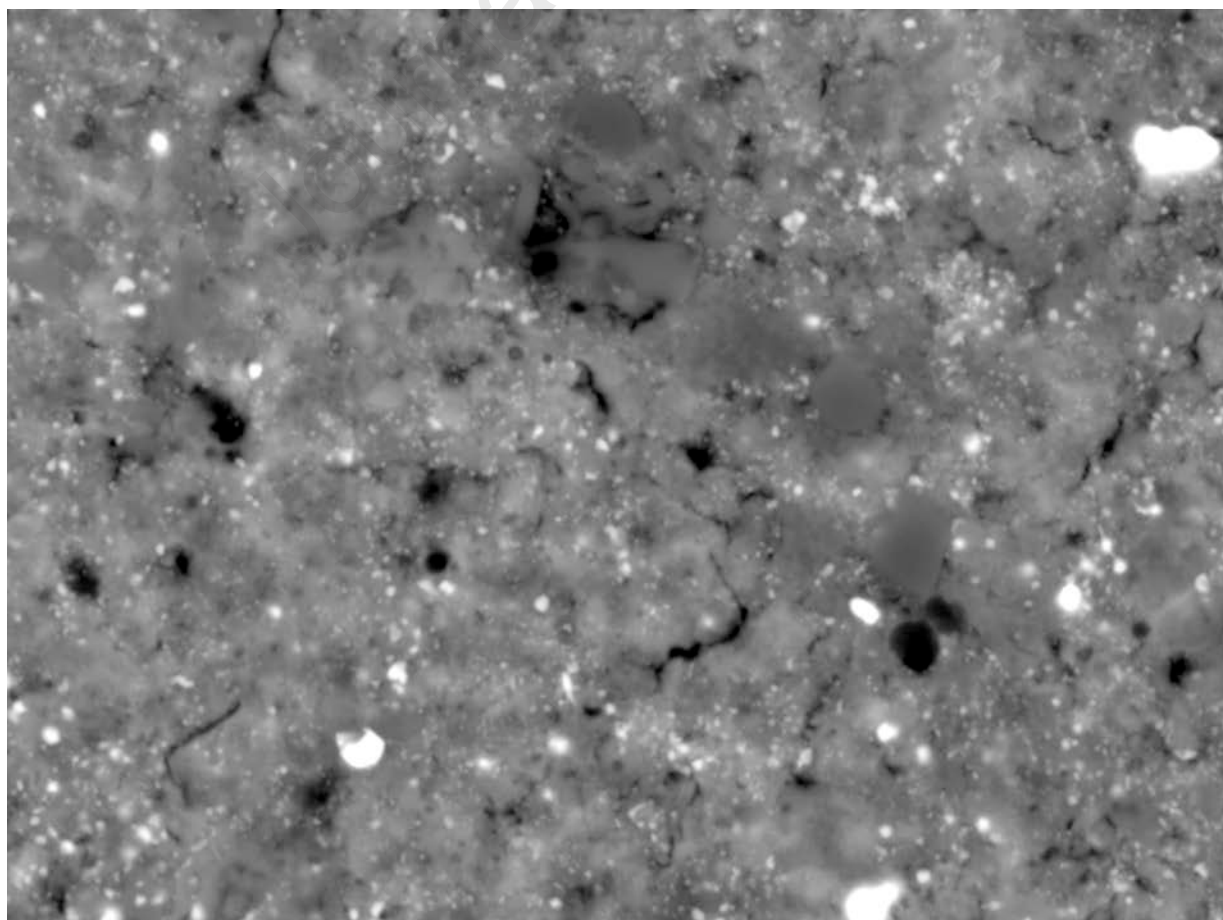


Fig. 2h

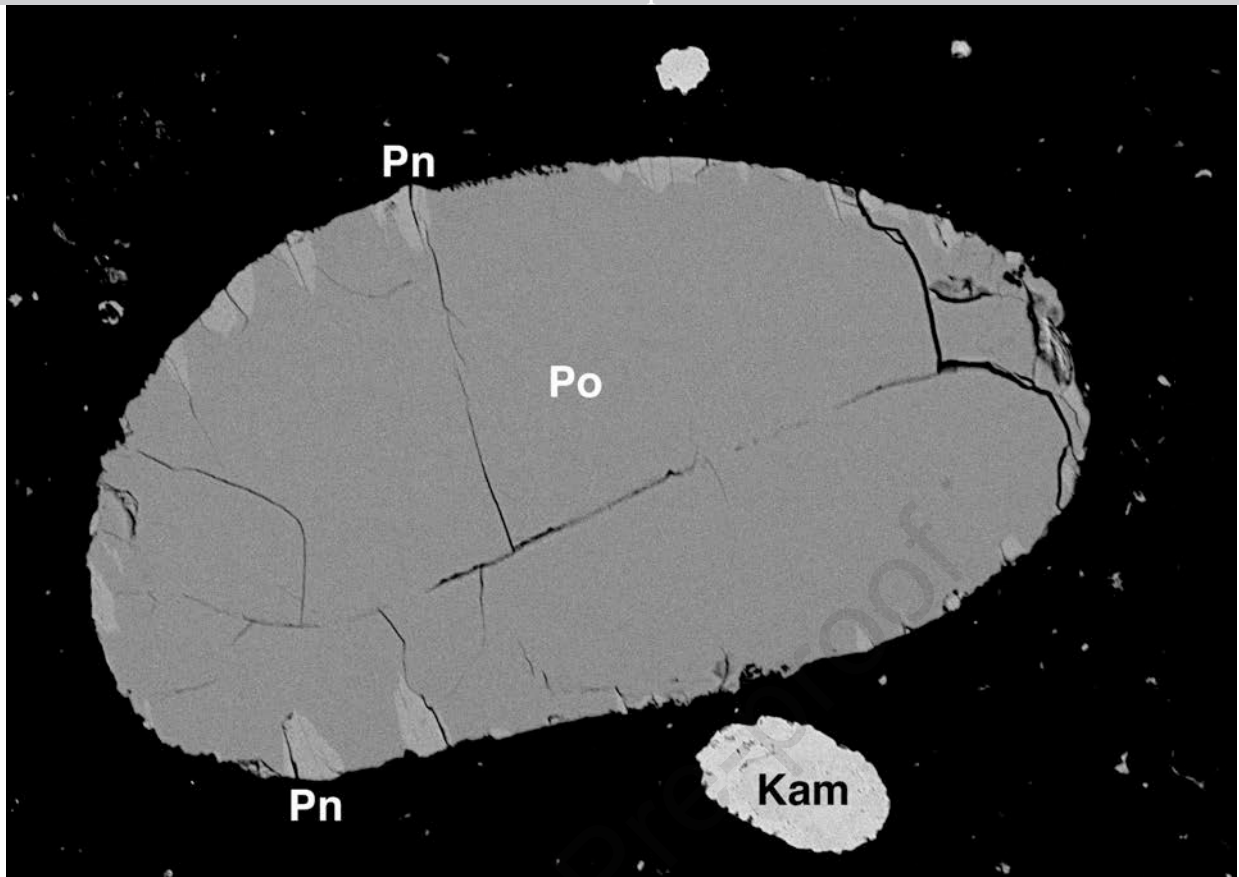


Fig. 2i

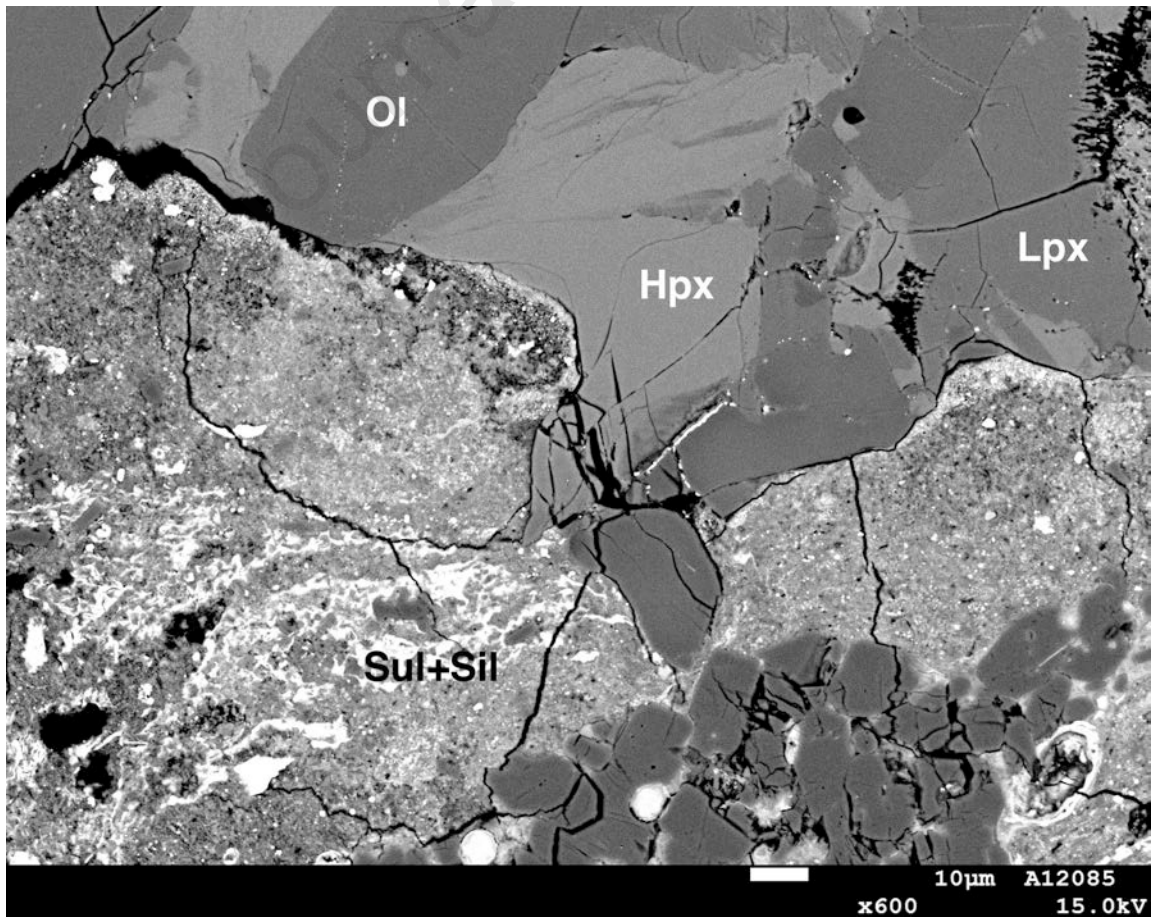


Fig. 2j

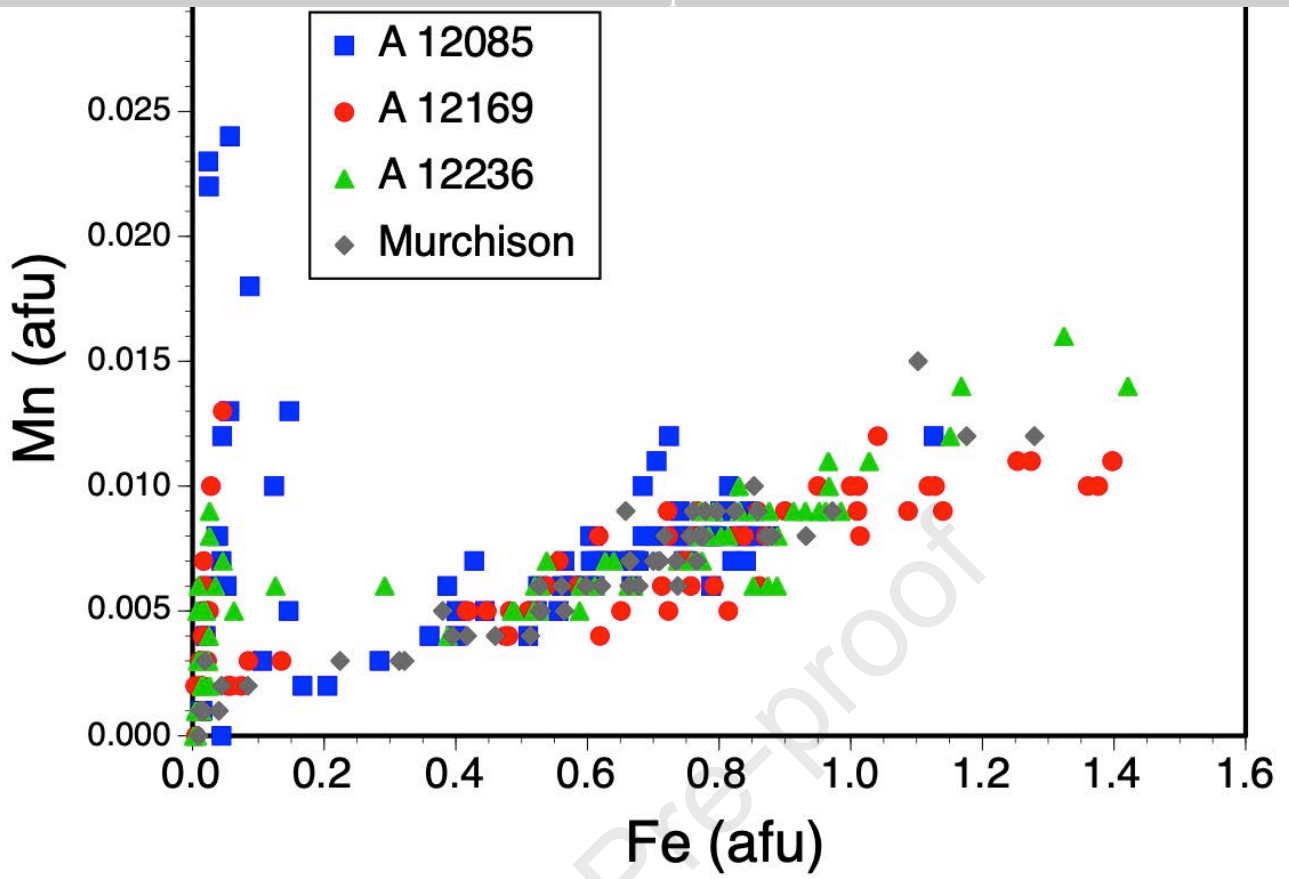


Fig. 3a

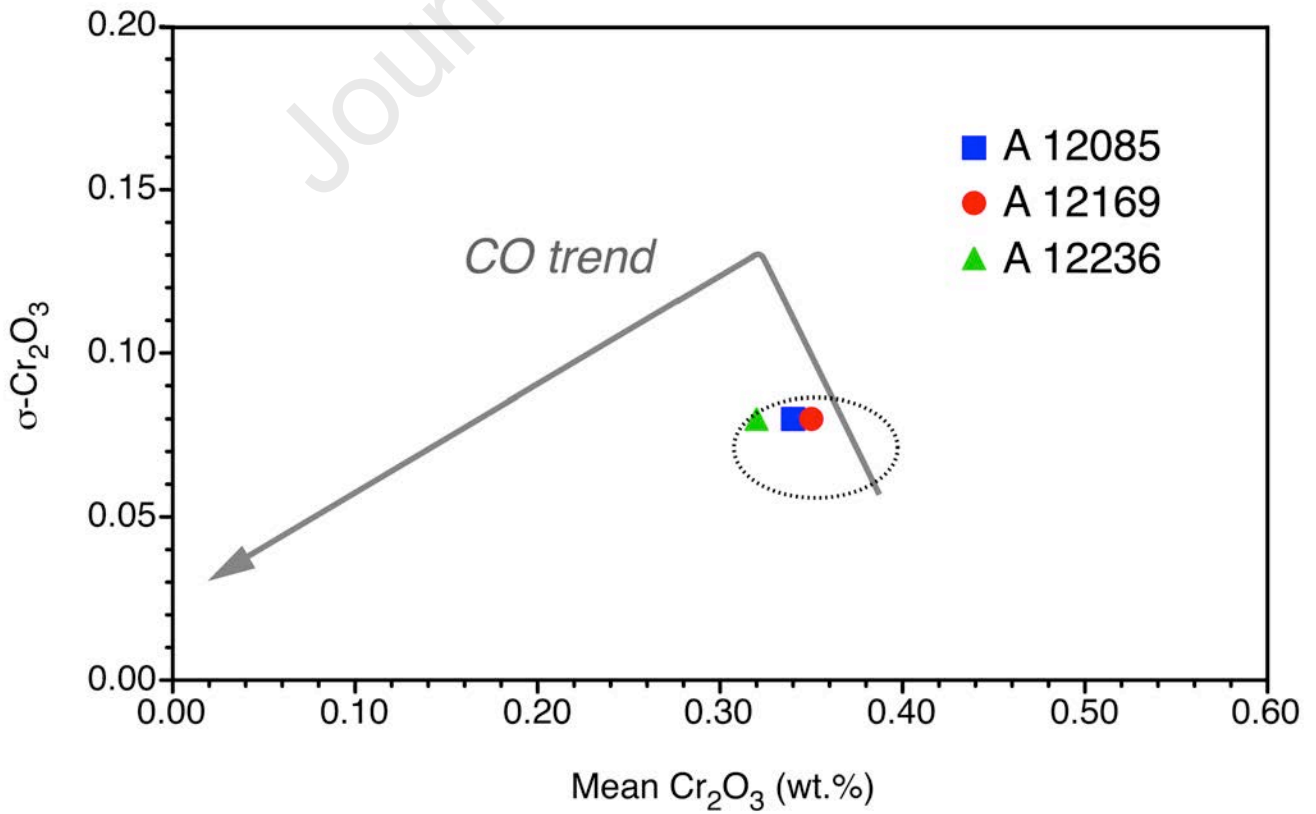


Fig. 3b

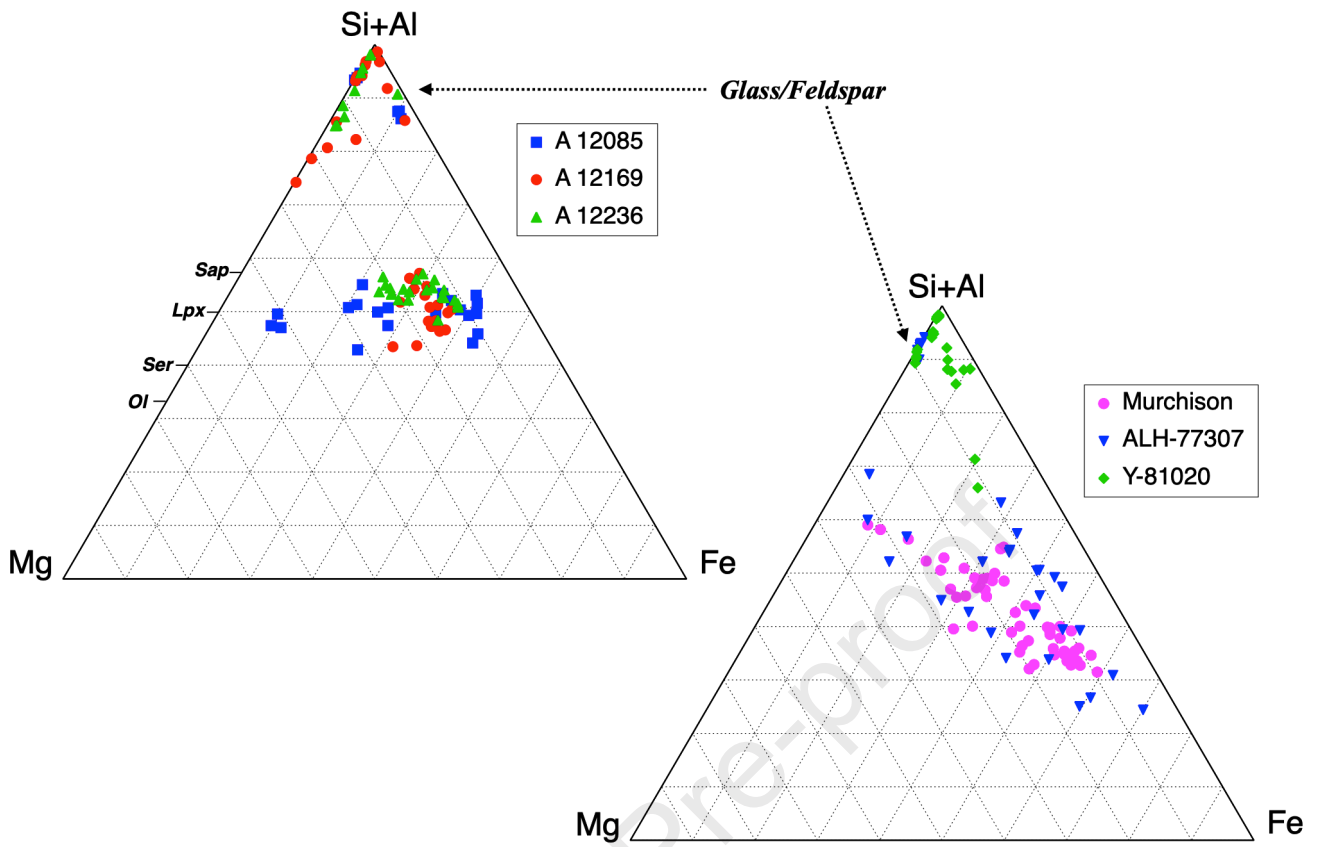


Fig. 4

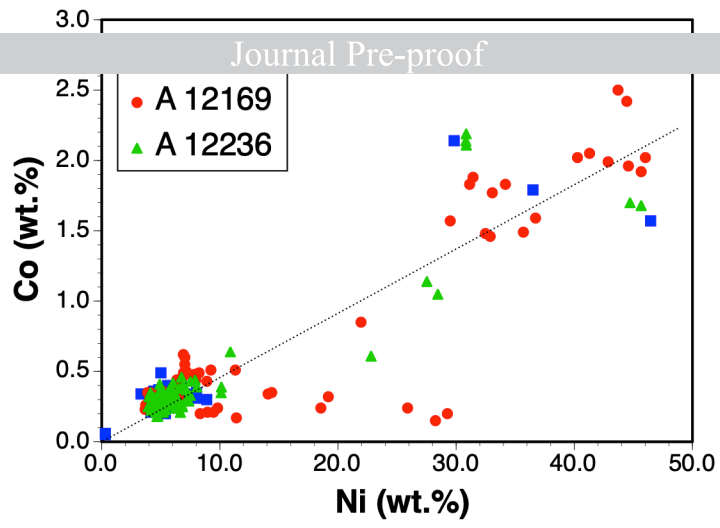


Fig. 5

Journal Pre-proof

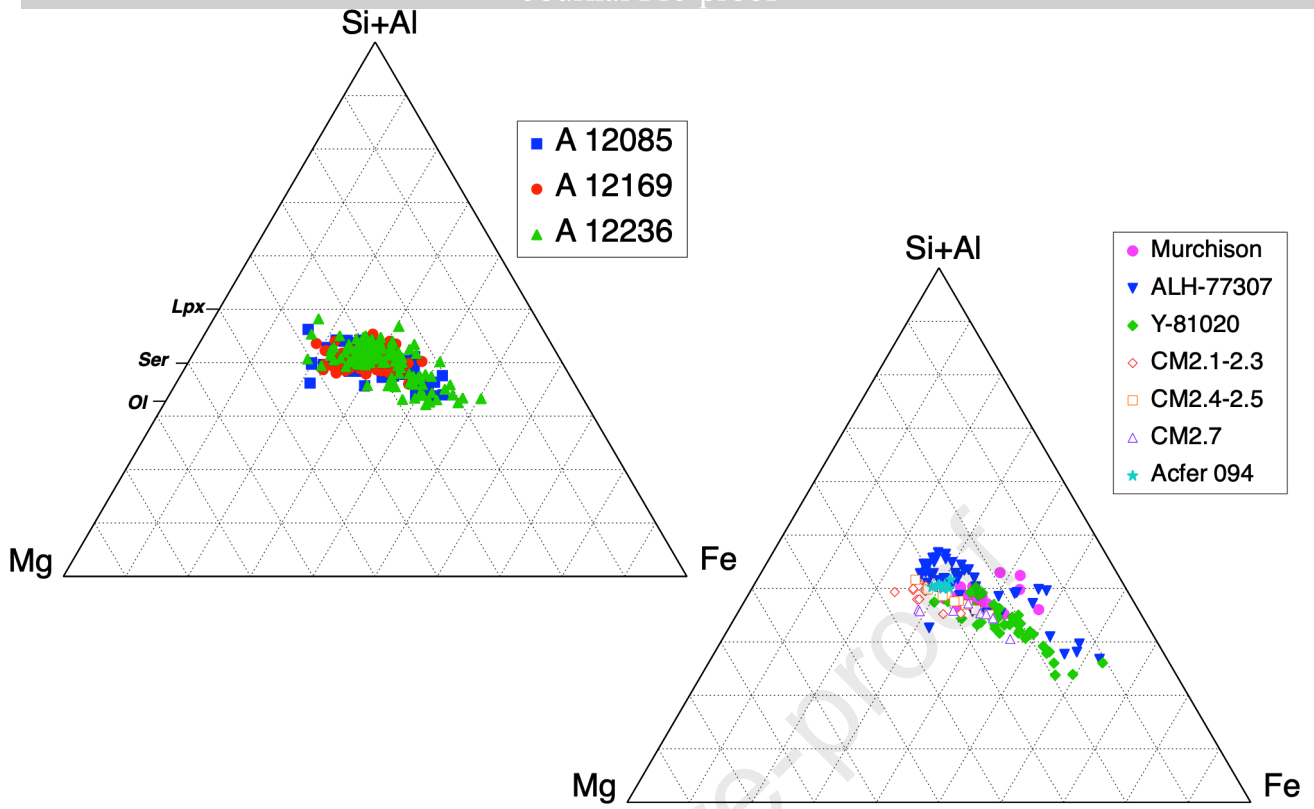


Fig. 6

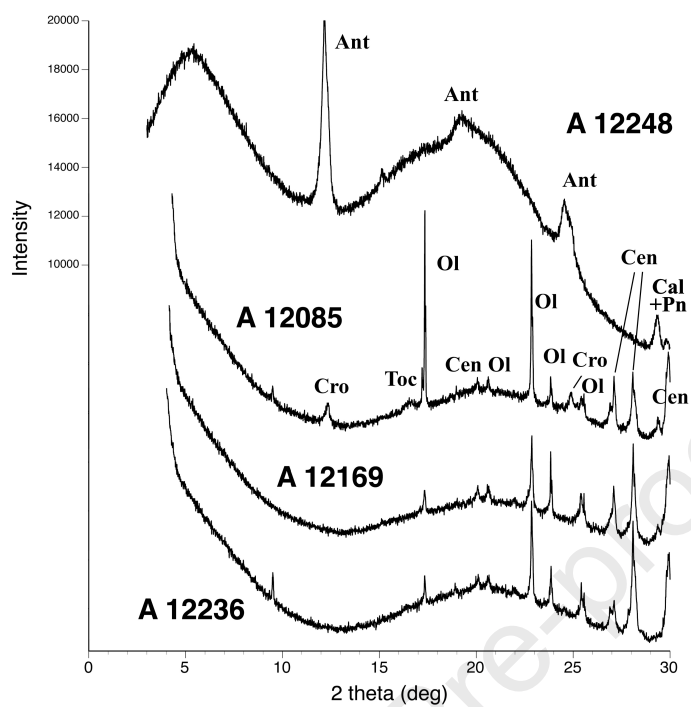


Fig. 7a

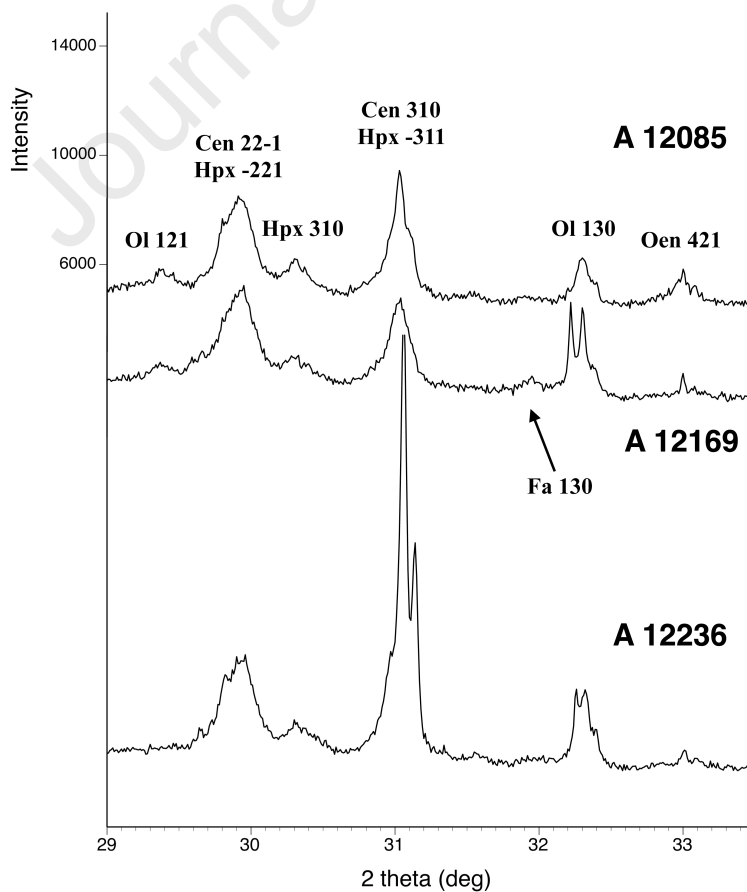


Fig. 7b

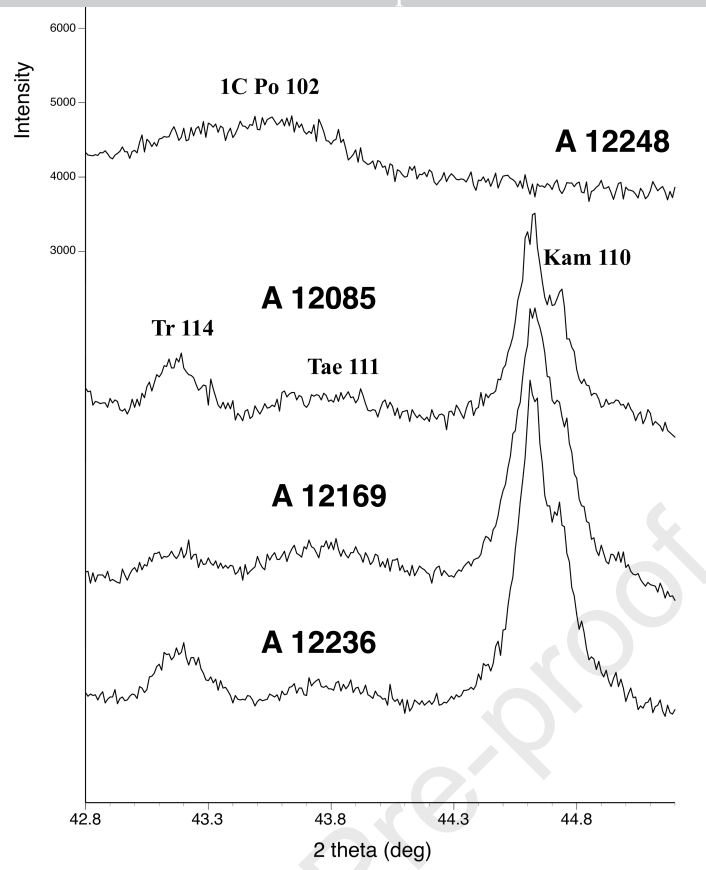


Fig. 7c

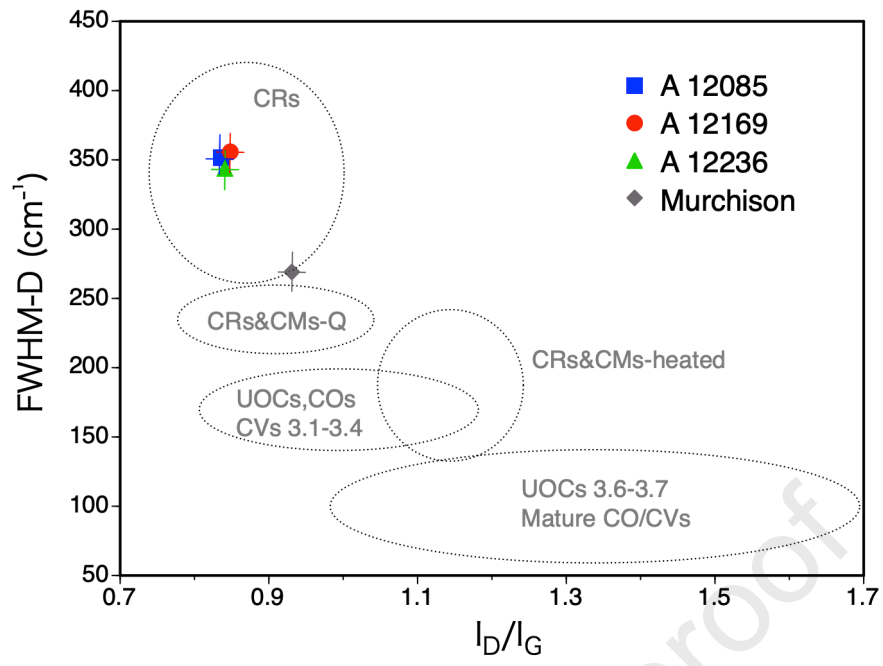


Fig. 8

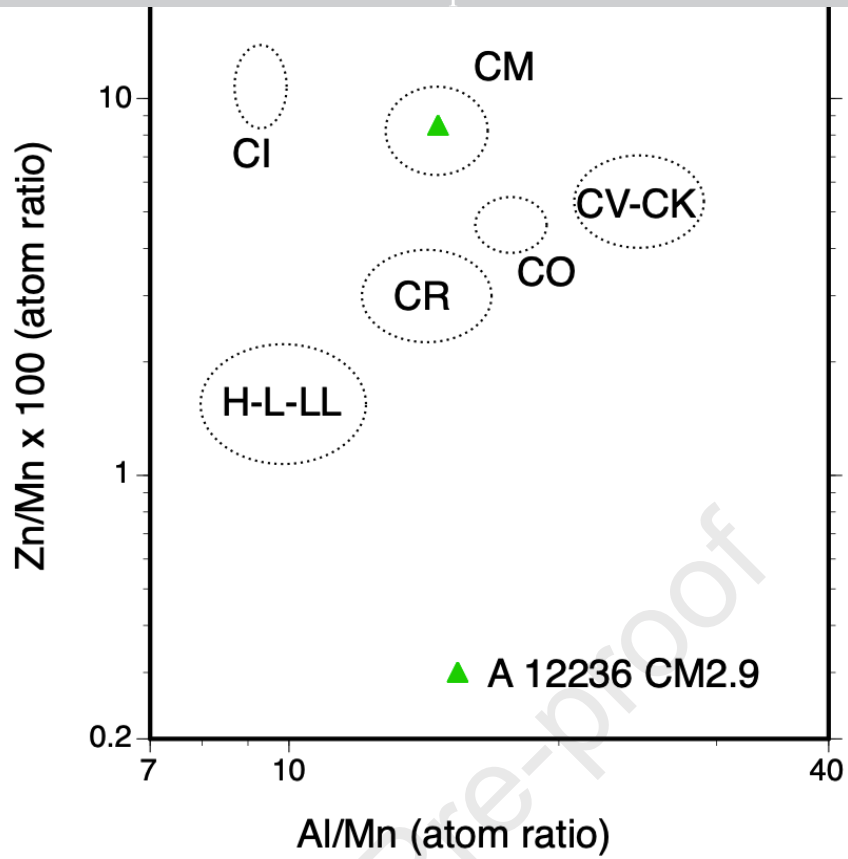


Fig. 9a

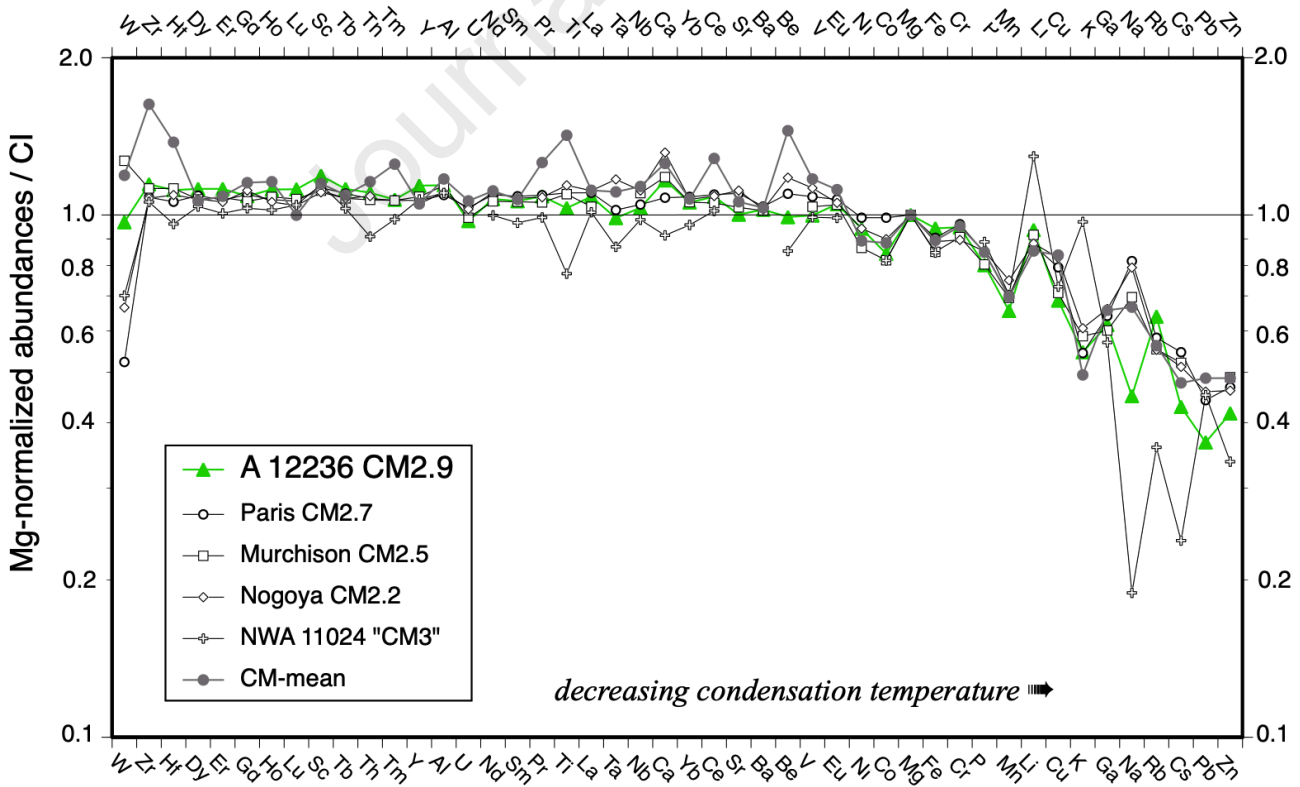


Fig. 9b